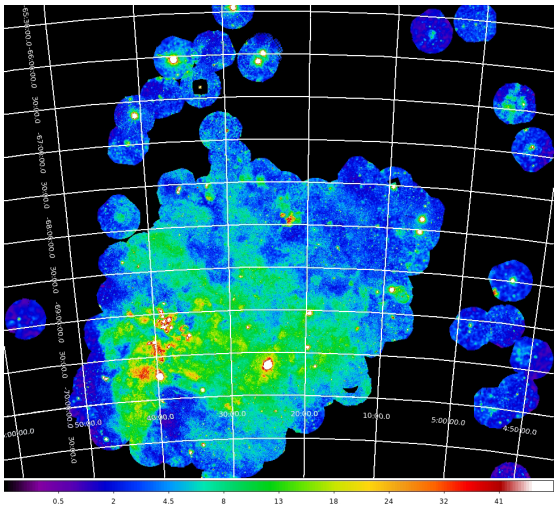

EPIC Mosaic of the LMC in the 0.4-1.3 keV band

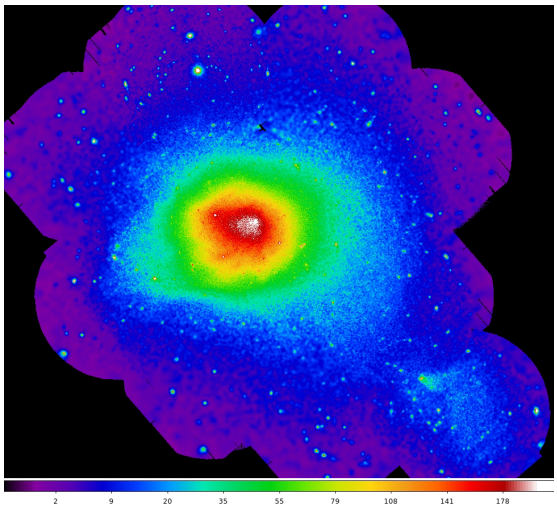

XMM Gallery EPIC mosaic of the Coma Cluster in the 0.4-1.3 keV band

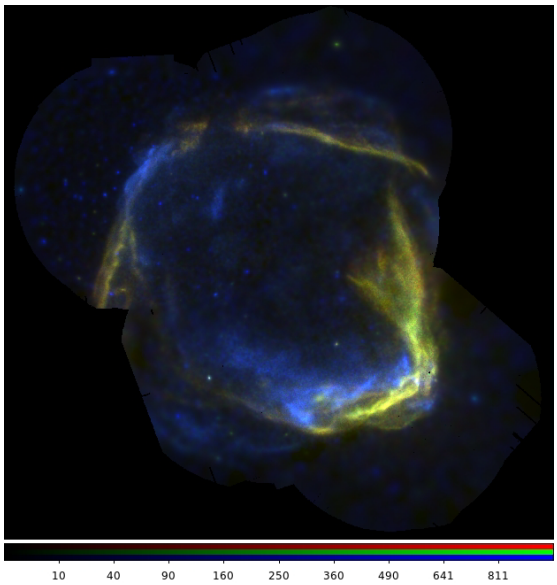

XMM Gallery EPIC false-color mosaic image of the SNR RCW86 with red: 0.4–0.75 keV, green: 0.75–1.3 keV, and blue: 2.0–7.2 keV

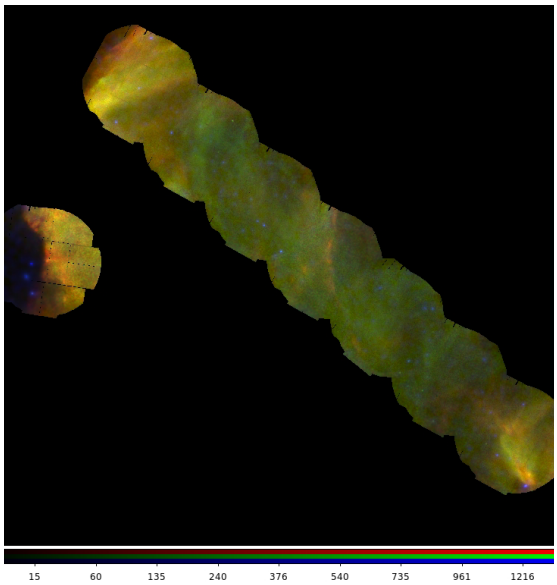

XMM Gallery EPIC false-color mosaic partial image of the Cygnus Loop SNR with red: 0.4–0.75 keV, green: 0.75–1.3 keV, and blue: 2.0–7.2 keV

XMM-Newton 2014 Senior Review Proposal

XMM-Newton Guest Observer Facility,
Guest Observer Funding, US RGS Hardware Team,
and XMM-Newton Education and Public Outreach

Prepared by: S. L. Snowden (NASA Project Scientist),
the US XMM-Newton Users Group (C. Sarazin, Chair),
the US Mission Scientist (R. Mushotzky),
and staffs of the US RGS Team and US XMM-Newton GOF

Contents

1 Science and Science Implementation 1
1.1 XMM Mission Attributes 1
1.2 Mission Overview 3
1.3 The Case for XMM-Newton 3
1.4 XMM-Newton Science 4
1.4.1 Active Galactic Nuclei (AGN) 5
1.4.2 Galaxy Clusters and the Dark Universe 8
1.4.3 Galaxies 9
1.4.4 Diffuse X-rays from the Milky Way and Solar System 11
1.4.5 Stars and Star Formation 12
1.4.6 Supernova Remnants (SNRs) 14
1.4.7 Neutron Stars (NSs) 15
1.4.8 X-ray Binaries 18
1.4.9 Cosmology, Surveys, and Serendipitous Science 19
1.5 Summary of Issues 20
1.6 Progress report and update to activities listed in the 2012 Senior Review proposal 21
1.7 Response to the 2012 Senior Review (SR) 21
1.8 Prioritized Mission Objectives (PMOs) 22
2 Technical and Budget 23
2.1 Observatory Operational Status 23
2.1.1 European Photon Imaging Cameras 23
2.1.2 Reflection Grating Spectrometers 23
2.1.3 Optical Monitor 23
2.2 NASA/GSFC Guest Observer Facility 24
2.2.1 GOF Services, Activities, and Current/Future Projects 24
2.2.2 Data, Data Distribution, and the Archive—Mission Archive Plan 26
2.3 Columbia University (CU) and the RGS 26
2.3.1 Previous Activities 26
2.3.2 Projected Responsibilities 27
2.3.3 The RGS Hardware Team 27
2.3.4 Guest Observer Grant Program 27
2.4 Education and Public Outreach (E/PO) 27
2.5 Budget Request Summaries 27
2.5.1 In-Guidelines Scenario 27
2.5.2 Optimal Augmented Budget Scenario 28
References 29
Appendix A. Standard Budget Spreadsheet 31
Appendix B. Acronyms 33
Appendix C. Online Bibliography 37

1 Science and Science Implementation

On behalf of the US Newton X-ray Multi-Mirror Observatory (XMM-Newton or XMM) user community, the NASA Goddard Space Flight Center (GSFC) Guest Observer Facility (GOF), the US Reflection Grating Spectrometer (RGS) Team, and the XMM Education and Public Outreach (E/PO) program, we request funding for the continued support of US participation in the European Space Agency (ESA) XMM mission. XMM's instruments provide a unique resource enabling US astronomers to produce high-quality and scientifically significant results with a particularly low cost to NASA relative to other Great Observatory-class missions.

XMM is the second cornerstone of the ESA Horizon 2000 program. Launched on 1999 December 10, XMM remains in full operation and in excellent health. ESA mission support is confirmed through 2014, with funding allocated through 2016.

1.1 XMM Mission Attributes

Relevance to NASA Goals: The science goals and achievements of XMM are directly responsive to the 2011 NASA Strategic Plan[1] Strategic Goal 2: "Expand scientific understanding of the Earth and the Universe in which we live," and through our E/PO effort Strategic Goal 6: "Share NASA with the public, educators, and students to provide opportunities to participate in our Mission, foster innovation, and contribute to a strong national economy." In addition, the XMM program is responsive to the Science Mission Directorate (SMD) 2010 Science Plan[2] providing important advances primarily towards the Astrophysics goal to "Discover how the Universe works, explore how the Universe began and developed into its present form, and search for Earth-like planets."

The 2010 Decadal Survey of Astronomy and Astrophysics[3] placed the next Great-Observatory class X-ray telescope (capable of replacing XMM and Chandra) fourth in the priority list with a launch in the 2020s. ESA's next X-ray mission, Athena+, has a suggested launch date no earlier than 2028. With a horizon of perhaps 15 years or more until the next mission launch capable of replacing XMM, the survival of an active and vibrant X-ray astrophysics community depends on maintaining US participation in the current missions as long as their instrumentation continues to function well. XMM provides exceptionally useful data to most areas of interest listed in the Decadal Survey with particular relevance to "The Physics of the Universe: Understanding Scientific Principles" and "Cosmic Dawn: Searching for the First Stars, Galaxies, and Black Holes." With its large collecting area and X-ray and optical/UV bands, XMM greatly facilitates studies of objects ranging from clusters of galaxies to compact objects, and their inherent physical attributes.

The Astrophysics Roadmap[4] lists three defining questions to be addressed in the next three decades. XMM is a world-class instrument for answering the third question, "How does the Universe work?" As we detail in this proposal, XMM enables investigations of the nature of the Universe. The X-ray Surveyor, the first notional observatory capable of superseding XMM in effective area and both spectral and angular resolution (although over a smaller field of view, FOV), is suggested for the "Formative Era," the second decade of the Roadmap. In the interim, the maintenance of a robust NASA XMM program is vital to enable science investigations supporting the roadmap's goals, and for the health of the US X-ray astrophysics community.

Science Applications: XMM provides crucial data for studies of fundamental and relativistic processes in neutron stars (NS) and quasars (e.g., constraining the spin of black holes in active galactic nuclei, AGN), the creation of the elements in supernovae (SNe) and their dispersal in supernova remnants (SNRs) and starburst galaxies, the evolution of the elements on the largest scales in groups and clusters of galaxies, and the distribution of dark matter in clusters, groups, and elliptical galaxies. XMM observations of young active stars provide important constraints on models of the early solar system and star forming regions, furthering understanding of the origin and evolution of the Sun and stars. While the science areas of XMM, Chandra, Suzaku, and Swift, and soon Astro-H, do overlap, XMM has unique capabilities that strongly enhance its utility to observers (see § 1.2).

Observatory Usage: XMM operates in a Guest Observer (GO) mode and the program is fully open to US participation, including US representation both in peer reviews and on the ESA Users Group. Announcements of Opportunity (AOs) are on an annual cycle with proposals due in October with a decision in December. In the most recent AO (AO-13) there were 452 proposals submitted with a time oversubscription of 5.4. Of those, 192 were approved. US scientists have been major participants in the GO

1 http://www.nasa.gov/pdf/516579main_NASA2011StrategicPlan.pdf
2 http://science.nasa.gov/media/medialibrary/2010/08/30/2010SciencePlan_TAGGED.pdf
3 http://www.nap.edu/catalog.php?record_id=12951
4 http://science.nasa.gov/media/medialibrary/2013/12/20/secure-Astrophysics_Roadmap_2013.pdf

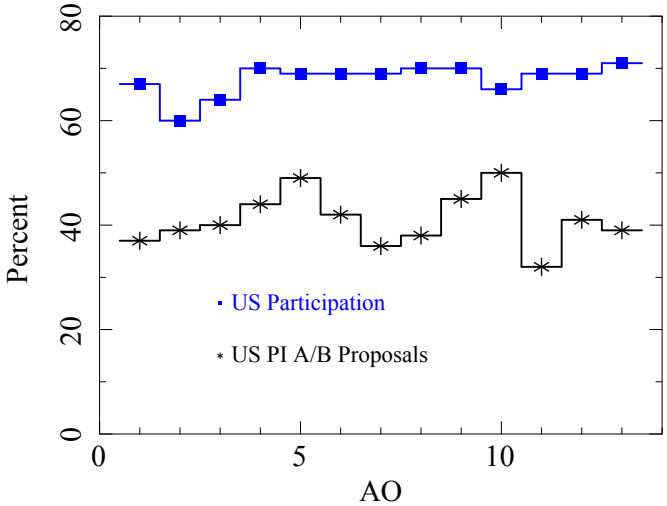

Figure 1. The high U.S. participation rates in accepted proposals by AO. The total rate includes A, B, and C (proposals with US PIs or Co-Is.

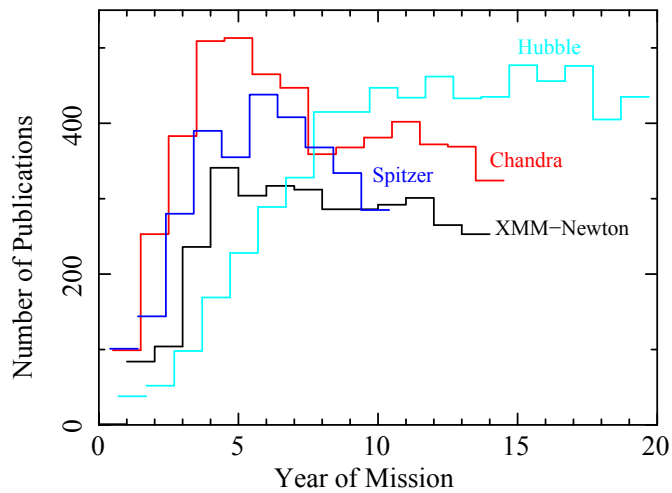

Figure 2. Comparison of XMM and other major observatory refereed publication rates versus year after launch. Publication numbers were taken from Astrophysics Data System (ADS) searches requiring the observatory's name to be in the paper's abstract or title, and to be included in the observatory's "group". This likely underestimates the total number of refereed papers (e.g., XMM papers are underrepresented by ~30%), but all missions are treated equally. ***XMM's publication rate is comparable to the other major observatories for a much smaller cost to NASA****.*

process through all AOs (Fig. 1). For AO-12 and AO-13, an average of 40% of the accepted proposals for A or B time (guaranteed observations) had US Principal Investigators (PIs). An additional 30% of the accepted A/B proposals had US Co-Investigators (Co-Is). There are typically ~250 targets chosen for guaranteed observation, with another ~250 targets chosen as "filler" observations (with a ~30% chance of being observed). The interest in XMM by the worldwide community remains high with a consistent time oversubscription. The project also accepts Target of Opportunity (ToO) requests with ~400 observed to date. As demonstrated by the large oversubscription factor, there is no obsolescence (perceived or actual) of the instruments.

Science Accomplishments: The major scientific achievements of XMM to date include: the solution of the decades-old "cooling flow" problem in clusters of galaxies; the unexpected detection of X-ray emission from brown dwarfs; the discovery of previously unknown types of novae and SNe; the observation of relativistic iron lines from NSs; the discovery of an ultra-luminous X-ray source (ULX, a probable intermediate mass black hole) in a globular cluster; the detection of the first quasi-periodic oscillation (QPO) in an AGN, connecting accretion by stellar mass and supermassive black holes; the discovery of the first binary NS which changes from a millisecond pulsar (MSP) to a low mass X-ray binary (LMXB), thus confirming the theory that LMXBs become MSPs; the detection of a virialized cluster of galaxies at z = 2.07; and detection of a filament of intergalactic gas between two clusters of galaxies, which may be evidence for the warm-hot intercluster medium (WHIM) containing most of the baryons in the present day Universe.

Scientific Productivity: The scientific output from XMM remains very strong with over 852 refereed papers in the last two years (25% have US lead authors and an additional 34% have US co-authors), and a grand total of 4519 through 2013 December (see Fig. 2 and the bibliography[5], this number is in excess of Fig. 2 as it is based on a detailed examination of the literature for a more complete bibliography). These papers are cited more often than the average refereed paper in the astronomical literature. Indeed, 43% of XMM papers published a year ago belong to the top 10% of the most cited articles published in the same time span, while 10% belong to the top 1%, a spectacular record of high-quality papers. In the last two years there have been four *Nature* papers and three *Science* papers based on XMM data, two of which had U.S. lead authors and five of which had U.S. co-authors.

NASA Support: NASA funds a GOF and a GO grant program to support the usage of XMM by the US scientific community. This includes providing proposal support, data analysis support, software development, calibration, hardware team, E/PO activities, and an archive. ESA bears the entire burden of mission operations allowing US expenditures to be relatively minor ($1.833 M in 2014) for access to data from a Great Observatory class mission.

5 http://heasarc.gsfc.nasa.gov/docs/xmm/xmmbib.html

Summary: XMM's status as one of the world's pre-eminent astronomical observatories is established by the high proposal oversubscription, high publication rate, and the frequent citation of refereed papers. Note that US scientists' impressive publication record for XMM comes with only limited GO funding support (we are able to fund only ~15% of successful US proposals) and without contributions from mission funded archive, theory, and fellowship opportunities that were available through the Chandra, Hubble, and Spitzer programs. With the continued high quality and health of instruments and satellite, the high proposal oversubscription rate, the large fraction of time going to US guest observers, the large archive, the rich scientific future, and the low cost to NASA, continued funding of the US XMM program is well justified.

Data Availability

XMM's observation data sets are made public after the expiration of a proprietary period, typically one year after data delivery. The XMM archive had 10,164 scientific observations (with a further 2,867 slew-survey observations) publicly available as of 2014 January.

1.2 Mission Overview

XMM observes in the 0.2–12 keV and optical/UV bands in a sky swath ±20° from the perpendicular to the Earth/Sun line. The observatory has three co-aligned high throughput 7.5 m focal length X-ray telescopes with 6″ full width at half maximum (FWHM) angular resolution. Three European Photon Imaging Camera (EPIC) charge-coupled device (CCD) detectors (PN, MOS1, and MOS2) provide X-ray imaging over a 30′ FOV with moderate energy resolution. XMM's imaging is complimentary to Chandra's, having larger effective area, broader bandpass, and larger FOV but with lower angular resolution. Compared to Suzaku, XMM has larger effective area, larger field of view, and better angular resolution, but somewhat poorer energy resolution and higher background. Higher resolution spectra ($E/\Delta E \sim 200$–800) are provided by two RGSs where gratings deflect half of the beam from two of the X-ray telescopes. These high spectral resolution instruments are capable of observing extended sources up to 2′ in extent. The RGS spectroscopic resolving power is intermediate between Chandra's grating spectrometers, but with significantly higher effective area. The sixth instrument, the Optical Monitor (OM), is a co-aligned 30 cm optical/UV telescope sensitive in the 1600–6500 Å band with a 16′ FOV and a wide variety of operational modes and filters. This simultaneous optical/UV imaging and spectroscopy is a capability shared only with Swift. XMM's two-day orbital period allows long, uninterrupted observations with contiguous coverage up to ~135 ks. This ability is critical for many timing studies of compact objects, for example, reverberation mapping in the X-ray band for AGN (i.e., the determination of the time lag of one X-ray spectral component relative to another).

Exceptional Instrumental Versatility

All of XMM's scientific instruments operate simultaneously, providing exceptionally rich data sets. All instruments can be run in a variety of modes, enabling them to be tuned for the scientific needs of specific investigations.

1.3 The Case for XMM-Newton

XMM excels in providing high throughput X-ray and optical/UV imaging, timing, and spectroscopy for an extremely wide variety of astrophysical sources, from comets and planets to quasars and clusters of galaxies. XMM provides this broad range of exceptional data to a large number of US GOs at a low cost to NASA.

There is no current mission, or any mission planned for launch in at least 15 years, which has XMM's combination of simultaneous high throughput X-ray imaging and spectroscopy, broad-band (X-ray, optical, and UV) capabilities, and ability to make long observations. The only relevant new mission is Astro-H, a Japanese-US mission that will have a spectroscopic capability superior to XMM's RGS above ~0.9 keV, but will not have the angular resolution or collecting area of XMM, or the ability to make long contiguous observations.

Because ESA and its member nations carry the costs for XMM operations, software development, and data processing, the US community has access to Great Observatory science at a small fraction of the cost to NASA of similar US-operated missions. The US community has received immediate access (either as PIs or Co-Is) to data from a steady ~70% of the total XMM programs (Fig. 1). While removing US XMM funding would not reduce the access of the US community to XMM's new observations, the lack of GO funding for data analysis and interpretation and the elimination of the US GOF science and technical support would have a significant impact on the productivity of the mission by reducing the US community participation. Continued funding will enable US scientists to maintain their leadership role in many of XMM's important discoveries in the coming years. GO funding support, absent in our "In-Guidelines" budget but comprising three quarters of our enhanced ("Over-Guidelines") budget request, combined with access to Astrophysics Data Analysis

Program (ADAP) funding, is vital to achieve the continued science output.

XMM is a general observation facility not closely linked to any specific field of astrophysical study, and is able to make observations supporting an extremely wide range of investigations. With its great flexibility and attributes, new ideas can be tested and, with the ToO program, XMM can be rapidly retasked (as fast as 5 hours but typically within 8 hours) to observe new phenomena. To increase the usefulness of XMM for ToOs from Fermi, Swift, and now NuSTAR, a new policy allows GOs to propose observations of targets whose coordinates are not known at the time of submission.

XMM excels at spectroscopic and timing follow-ups to new ground and space-based surveys, such as the Planck cluster survey. XMM's capabilities in the X-ray and optical/UV bands coupled with NuSTAR's 3–79 keV bandpass, sensitivity, and imaging ability are making possible exceptionally detailed studies of faint black holes, mapping the Galactic center region in hard X-rays, imaging supernova remnants and mapping their radioactive elements, and monitoring blazars. Indeed, in AO-13 62 proposals for joint XMM/NuSTAR observations were submitted, and 18 accepted.

ESA modified the XMM AO to introduce proposals for very large programs (VLPs) allowing requests for 1–3 Ms of time, and increasing the time dedicated to large programs (LPs) and VLPs to about 30% of the total. This has allowed investigations, which, because of their required exposures, were not approved in early AOs. Examples include the deep surveys of the Large and Small Magellanic Clouds (LMC, SMC), M31, and M33 that are enabling very sensitive studies of their X-ray source populations and diffuse emission. XMM also pursues cutting-edge high risk/high reward observations.

XMM's Unique Properties Ensure a Bright Future

1) The large effective area enables studies requiring many counts (but not necessarily high count rates) such as determining the abundance profiles of high-z clusters, or the structure of AGN Fe K lines, allowing the determination of black hole spin.
2) The ability to make long continuous observations enables studies requiring long-looks, such as AGN timing or detailed studies of isolated neutron stars.
3) The combination of X-ray and Optical/UV bandpasses support studies requiring multi-wavelength observations, such as detailed studies of star forming regions.
4) XMM's large grasp (effective area-solid angle product), and therefore reduced exposure requirements, enable projects needing large samples of objects (e.g., legacy programs), such as studies of groups of galaxies.
5) The ability to obtain good signal-to-noise (S/N) spectra for weak sources supports studies such as the origin of the X-ray background and binary populations in nearby galaxies.
6) The wide FOV and project software allows studies of extended sources requiring the mosaicking of pointings such as the diffuse X-ray background, SNRs, nearby galaxies, and clusters of galaxies.

XMM has a rich scientific future and US astrophysicists, with continued scientific funding and technical/analysis support from the GOF, can be expected to remain outstanding participants in the program.

1.4 XMM-Newton Science

Exciting new discoveries by XMM are suggested by the LPs in AO-12 and AO-13, over half of which have US participation. These projects will provide US astronomers with immediate access to a wealth of astrophysical data. The AO-12 and AO-13 LPs with US involvement include:

1) A detailed X-ray study of CoRoT2a, the most active planet host-star known, to determine the effect of early stellar activity on planets. X-ray transits will be used to search for planetary "blow-off".

2) A coordinated X-ray/radio campaign on the best-studied mode-switching radio pulsar, PSR B0943+10, to determine the magnetic geometry and emission mechanisms.

3) The mixed-morphology SNR W44 was recently discovered to have considerable amounts of over-ionized plasma. (SNRs are typically under ionized due to their young age.) The location of this material will be derived in 3D in the SNR.

4) Absorption measurements from a series of pointings at the southern terminus of the North Polar Spur will be used to determine whether it is part of the Loop I superbubble (roughly centered on the Sco-Cen OB association), or a supershell centered on the Galactic center.

5) A search for extended hot coronae around massive, rapidly rotating spiral galaxies.

6) Determining the nature, energetics, and location of the AGN outflow in NGC 5548, as has recently been done with Mrk 509 (§ 1.4.1 and Fig. 5 below). This is a multi-wavelength campaign including Hubble Space Telescope (HST), Swift, and ground-based optical observations.

7) Mapping the inner accretion disk wind in the nearby quasar PDS 456 from roughly 10 to 100 Schwarzschild radii.

8) A deep X-ray view of the "bare nucleus" Seyfert galaxy Ark 120 to determine properties of the accretion disk and the black hole spin.

9) A spectroscopic study of 11 groups and clusters of galaxies to determine their chemical enrichment mechanisms and history.

10) A study of the Sculptor Wall (z = 0.33) X-ray absorber to search for OVII Kα and Kβ; the latter would establish this as WHIM-like plasma, rather than as a galactic halo.

11) The XMM-ATLAS survey to follow up the Herschel-ATLAS 16 deg^2 survey in X-rays.

12) An X-ray survey of Sloan Digital Sky Survey (SDSS) Stripe 82 to determine supermassive black hole growth in quasars.

13) Continuation of the huge Extra Extra Large (XXL) 50 square degree extragalactic survey.

The future science of XMM is considerably enhanced by the availability of the well-calibrated and extensive EPIC Serendipitous Source Catalog and associated data products (3XMM-DR4, see Fig. 17), EPIC Slew Survey Source Catalog (SSSC), and OM Catalog (OMCat, produced by the US GOF). These databases are invaluable resources for archival research and, in addition, provide finding charts for future proposals. The science proposed for XMM is often based on past observations, both where objects are re-observed with deeper exposures after preliminary survey observations, and where the target is expected to have long-term temporal variations.

Continual improvements in calibration and the advent of new software allow measurements, for example, of the soft X-ray background, Galactic plane emission, and measurement of the mass profiles of clusters. The continued development of the XMM Science Analysis System (SAS) has made analysis easier and more robust as well as providing new automatic data products, easing the analysis of the large and complex data sets.

Demonstrating the wealth of XMM discoveries in the last two years requires focusing on a small representative fraction of the results. The following is just a taste of what has been accomplished since the last Senior Review.

1.4.1 Active Galactic Nuclei (AGN)

XMM has provided a revolutionary and unique view of AGN over the last decade, and this science continues to be a cornerstone of the mission's portfolio. XMM's superior effective area enables it to collect spectra with higher signal-to-noise ratios in a given time than any other current X-ray observatory, and its orbit enables long continuous observations. Combined, these two properties make XMM ideal for deep exposures of AGN, which can vary in flux by up to an order of magnitude in a matter of hours. Further, the simultaneous data collected by the EPIC, RGS and OM instruments allows astronomers to examine self-consistently the properties of the absorbing gas/outflowing wind, continuum, distant and inner disk reflection, and soft excess. In the past two years, XMM has also been utilized with higher-energy observatories such as NuSTAR and INTEGRAL to obtain simultaneous, broadband data over the full X-ray range. Such data paint a more complete picture of the correlations between spectral components, enabling us to more accurately assess their origins and physical properties.

Relativistic Reflection and Black Hole Spin: In principle, one can measure the spin of the supermassive black hole (SMBH) at the AGN's core by properly characterizing the degree to which the reflection spectrum is shaped by relativistic effects from the innermost regions of the accretion disk proximal to the event horizon. In practice, however, separating these spectral signatures from the surrounding continuum and complex absorption intrinsic to most AGN has been an ongoing challenge. Though the existence of relativistic, inner disk reflection features in AGN has been argued since the seminal work of Tanaka et al. (1995, using ASCA to observe MCG-6-30–15), the controversy over whether the data can be fit equally well with a superposition of partial-covering absorption components has been continually revisited. It has become clear that broadband, very high S/N data are necessary to break this modeling degeneracy.

Risaliti et al. (2013) employed XMM and NuSTAR simultaneously to observe the Seyfert 1.9 galaxy NGC 1365 four times from July 2012 to February 2013, with the goal of tackling this issue in a source with a well-known, variable neutral absorber, an ionized absorber, and putative relativistic reflection signatures. Though these four pointings caught the source with very different absorbing columns, ranging from $N_H=10^{22}$–10^{24} cm^{-2}, the remaining spectral feature was virtually identical in each case once the continuum and absorption were modeled out (Risaliti et al. 2013, Walton et al. 2013, submitted). Further, modeling the XMM-only data with a relativistic reflection or multiple partial-covering absorber components was equally effective, but combined with NuSTAR the data showed an overwhelming preference for the reflection model above 10 keV (Risaliti et al. 2013, Fig. 3). The spin of the black hole measured from these observations is a>0.97, essentially the maximum that can result from disk accretion.

Done et al. (2013) constrained black hole spin in a sample of narrow-line Seyfert 1 (NLS1) galaxies through a method complementary to relativistic reflection modeling: fitting the thermal disk continuum

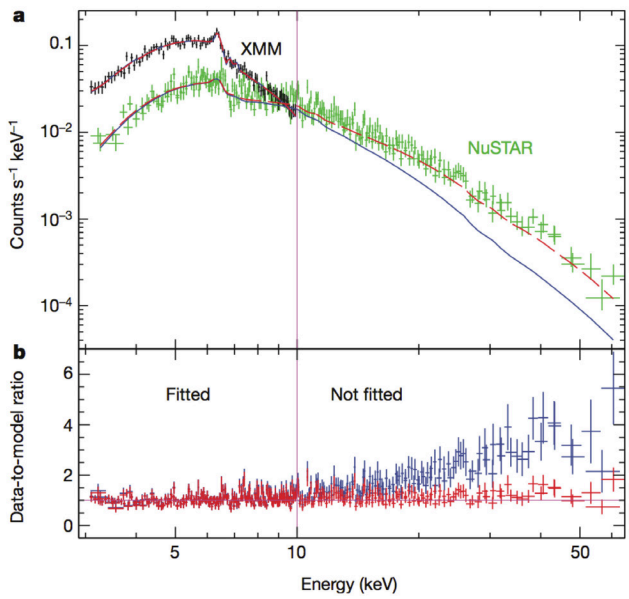

Figure 3. Spectrum of the first simultaneous XMM/NuSTAR observation of NGC 1365, which is fit equally well below 10 keV with a model including relativistic reflection or multiple partial-covering absorbers. The models diverge significantly above this energy, however, with relativistic reflection being clearly a better fit to the data (Risaliti et al. 2013).

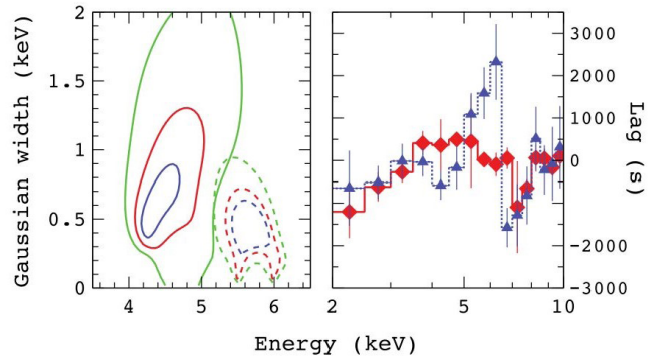

Figure 4. Results from the XMM observation of the Fe K line reverberation time lags in the Seyfert 1.5 galaxy NGC 4151 (Zoghbi et al. 2012). Left: Confidence contours for the width and energy of the Gaussian lines fitted to the lag spectra. The dashed and continuous lines are for temporal frequencies of < 2 x 10^{-5} Hz and (5-–50)x10^{-5} Hz, respectively. The contours represent 90%, 95%, and 99% limits shown in blue, red, and green, respectively. Right: Lag-energy plots taken at different temporal frequencies where larger frequencies represent smaller radii in the disk. The blue triangles are for < 2 x 10^{-5} Hz and the red diamonds are for (5–50) x 10^{-5} Hz.

in X-rays in order to determine the radius of the innermost stable circular orbit. This technique has hitherto been used predominantly in stellar-mass black holes (e.g., Remillard & McClintock 2006). The authors apply the technique to the NLS1 PG 1244+026, where the optical/UV/X-ray spectrum is consistent with being dominated by a standard disk component. This gives a best estimate for black hole spin at a < 0.86, in contrast to the recent X-ray determinations of (close to) maximal black hole spin in other NLS1 based on relativistic smearing of the iron profile. If this method for measuring spin in disk-dominated AGN is shown to be robust in multiple sources, it will provide an important new means through which to perform this science and would enable the sample size of AGN SMBH spins to increase significantly.

Fe K Reverberation Time Lags: Zoghbi et al. (2012) reported the first detection of reverberation in the Fe K band in an AGN. Using XMM observations of NGC 4151, the authors found delays of the order of 2000 s on timescales of 10^5 s between the 5–6 keV band vs. the 2–3 keV and the 7–8 keV bands, with a broad lag profile resembling a relativistically broadened iron line. The peak of the lag spectra shifts to lower energies at higher frequencies, consistent with emission of the red wing of the line at smaller radii, as expected for reflections from the inner accretion disk (see Fig. 4). Zoghbi et al. (2013) performed a similar analysis of XMM data from MCG-5-23-16 and NGC 7314; in both objects, lags between energy bands were found with a time delay of ~1 ks. These lags are fully consistent with reverberation of the relativistically broadened Fe Kα line. The measured lags, their timescale, and their spectral modeling indicate that most of the radiation is emitted within ~5 and 24 gravitational radii for MCG-5-23-16 and NGC 7314, respectively.

Investigating reverberation-induced time lags in a sample of AGN rather than focusing on individual sources, De Marco et al. (2013) carried out a systematic analysis of time lags between X-ray energy bands in 32 unabsorbed, radio-quiet AGN observed by XMM. The authors report that a total of 15 out of 32 sources display a high-frequency soft lag in their light curves (97% confidence). The frequencies in which the lags are seen are comparable with those found by Zoghbi et al. above, and the DeMarco et al. work also supports the correlation between mass, lag frequency, and amplitude noted by Kara et al. (2013): soft lags are systematically shifted to lower frequencies and higher absolute amplitudes as the mass of the source increases. These results strongly suggest the existence of a mass-scaling law for the soft/negative lag that holds for AGN spanning a large range of masses (about 2.5 orders of magnitude), thus supporting the idea that soft lags originate in the innermost regions of AGN and are powerful tools for testing their physics and geometry.

Absorption in the Central Engines of Active Galaxies: Absorption intrinsic to the galactic nucleus complicates the spectra of many AGN. This absorbing gas is traditionally observed to be neutral

and/or partly ionized, sometimes altering the shape of the spectrum in the Fe K band. While neutral absorption is usually observed in the rest-frame of the AGN, significant outflow velocities have been associated with many highly ionized absorbers.

Tombesi et al. (2012) examined blueshifted Fe K absorption lines in a sample of 42 local radio-quiet AGNs observed with XMM, estimating the location and energetics of the associated ultrafast outflows (UFOs). On average, the authors found their location is in the interval ~10^2–10^4 Schwarzschild radii from the central black hole, consistent with the expectation for accretion disc winds/outflows. The mass outflow rates correspond to 5–10% of the accretion rates. The minimum possible value of the ratio between the mechanical power and bolometric luminosity is constrained to be comparable or higher than the minimum required by simulations of feedback induced by winds/outflows, demonstrating that UFOs are indeed capable of providing a significant contribution to cosmological feedback.

Pounds & King (2013) reported on an extended XMM observation of the Seyfert 1 galaxy NGC 4051 taken in 2009, which revealed an unusually rich absorption spectrum with outflow velocities, in both RGS and EPIC spectra, up to ~9000 km s^{-1}. Evidence was again seen for a fast ionized wind with a velocity of v~0.12c. Detailed modeling with the XSTAR photoionization code now confirms the general correlation of velocity and ionization predicted by mass conservation in a Compton-cooled shocked wind. The authors conclude that the 2009 observation of NGC 4051 gives strong support to the idea that a fast, highly ionized wind, launched from the vicinity of the supermassive black hole, will lose much of its mechanical energy after shocking against the ISM at a sufficiently small radius for strong Compton cooling. However, the total flow momentum will be conserved, retaining the potential for a powerful AGN wind to support momentum-driven feedback. In this scenario, the warm absorber components often seen in AGN spectra may result from the accumulation of shocked wind and ejected ISM.

Multi-Wavelength Observations and Surveys: Though the power of using XMM in conjunction with observatories at other wavelengths has been touched on earlier in this section, the true capabilities and assets of the mission are uniquely highlighted by its contributions to deep, multi-wavelength observing campaigns on AGN, either as single objects or in broader surveys comprising hundreds or thousands of sources.

Petrucci et al. (2013) examined the XMM and INTEGRAL data from the Mrk 509 campaign and, prompted by the correlation between the UV and soft X-ray flux, they determined that the presence of a relatively hard high-energy spectrum points to the existence of a hot (kT~100 keV), optically-thin (τ ~ 0.5) corona producing the primary continuum (see Fig. 5). In contrast, the soft X-ray component requires a warm (kT ~ 1 keV), optically thick (τ ~ 10–20) plasma. Estimates of the amplification ratio for this warm plasma support a configuration relatively close to the theoretical configuration of a slab corona above a passive disk. An interesting consequence is the weak luminosity-dependence of its emission, which is a possible explanation of the roughly constant spectral shape of the soft X-ray excess seen in AGNs. The temperature (~3 eV) and flux of the soft-photon field entering and cooling the warm plasma suggests that it covers the accretion disk down to a transition radius of R_{in}=10–20 gravitational

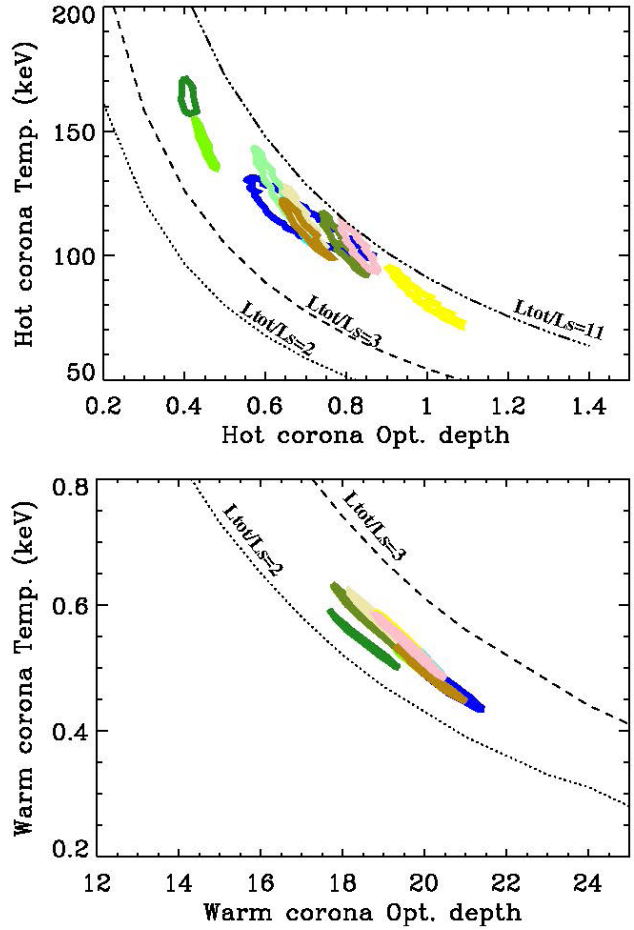

Figure 5. Contour plots of the temperature versus optical depth for the hot (top) and warm (bottom) accretion disk corona for the 10 observations (indicated by different colors) of Mrk 509 (Petrucci et al. 2013). A steady state with a soft-photon temperature of 10 eV is assumed, and different Compton amplification ratios are overplotted. Dotted line: L_{tot}/L_s=2; dashed line: L_{tot}/L_s=3; dot-dot-dot-dashed: L_{tot}/L_s=11. Here, the amplification ratio gives the total Compton plus soft radiation luminosity L_{tot} divided by the soft radiation luminosity L_s.

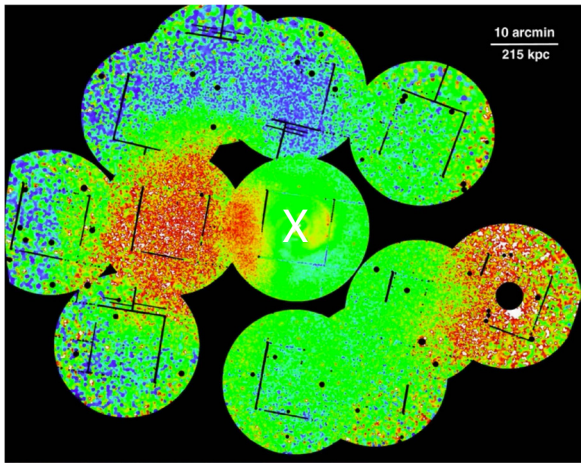

Figure 6. Residual XMM mosaic of the Perseus cluster after dividing the image by the azimuthal average of the cluster emission (Simionescu et al. 2012). Significant residuals exist ~1 Mpc from the cluster center (white "X") both to the east and west of the cluster. Spectral fitting indicates that the feature to the east is a cold front, one of only two ~1 Mpc off-axis cold fronts discovered to date.

radii. In contrast, the hot corona has a more photon-starved geometry. The high temperature (~100 eV) of the soft photon field entering and cooling it favors a localization of the hot corona in the inner flow. In this framework, the change in the geometry (i.e., R_{in}) could explain most of the observed flux and spectral variability.

1.4.2 Galaxy Clusters and the Dark Universe

New inroads into understanding galaxy cluster physics continue to be made with XMM. The presence of sloshing cold fronts in clusters which result from a perturbation in the gravitational well of a cluster brought about by an off-axis minor merger was an unexpected discovery of the last decade. While initially considered to be a phenomenon associated with the inner regions of clusters, recent XMM imaging of the outer regions of Perseus (Simionescu et al. 2012) and Abell 2142 (Rossetti et al. 2013) have identified sloshing features at radii approaching 1 Mpc from the cluster centers (Fig. 6). Sloshing features at such large radii are not predicted by current numerical simulations, and, if confirmed in other clusters, will have important ramifications for our understanding of how even minor mergers can significantly affect the global properties of clusters.

Given that clusters of galaxies represent the largest gravitationally bound systems in the Universe, their baryon fractions should approach the cosmological value of $f_b \approx 0.17$. A careful determination of the total baryon content of a cluster, including the difficult-to-measure intracluster stellar light profile, is necessary to accurately obtain f_b. Sanderson et al. (2013) analyzed XMM observations of five ***optically-selected*** low mass clusters chosen to have well-determined intracluster light profiles to derive the stellar, gas, and total baryon fraction for comparison at r_{500}, where the average interior total density (baryons plus dark matter) is equal to 500 times that of the critical density of the Universe at the cluster redshift. They found that the baryon fractions at r_{500}, for four of these five clusters, were systematically lower than that found in more massive clusters. Given that AGN feedback and cooling is expected to be more prevalent in lower mass clusters, the "missing" baryons could conceivably have been pushed out to even larger radii by these processes, motivating the need for future X-ray observations to radii beyond r_{500}.

Churazov et al. (2012) combined deep XMM (Fig. 7) and Chandra pointings of the Coma cluster to analyze X-ray surface brightness fluctuations in Coma's intracluster medium (ICM). They constructed a two-dimensional power spectrum of the de-

Future AGN Research

In AO-12 and AO-13, seven long observing programs were accepted in the field of AGN research: multi-wavelength monitoring of NGC 5548 (similar in scope to the campaign on Mrk 509 described above), mapping of the inner accretion disk wind in PDS 456, a joint XMM/Chandra High Energy Transmission Gratings (HETG) observation to probe the soft excess in Ark 120, observations of the ultra-fast out-flow wind in the Seyfert galaxy PG1211+143, a reverberation analysis of the simple spectrum narrow-line Seyfert 1 galaxy PG 1244+026, an X-ray survey of SDSS Stripe 82 to determine supermassive black hole growth in quasars, and a multi-wavelength survey using XMM, Herschel, UKIDSS and WISE to probe the link between AGN and star formation in the local Universe and to investigate the effects of very luminous AGN on their galactic hosts. Results from each of these projects will be forthcoming during the next two years.

Further proposals are likely to capitalize on XMM's unique flexibility in performing simultaneous observations (X-ray and optical/UV) with other missions, including studies of AGN that will involve NuSTAR, HST, Swift, and other instruments. The areas of study described above will continue to be priorities, carrying on the considerable rate of advancement in these fields that has been enabled by XMM over the past decade. The continuing efforts of the mission to facilitate long and/or coordinated observations will strengthen its legacy and continue to enrich its archives, assuring a long-term benefit to the community.

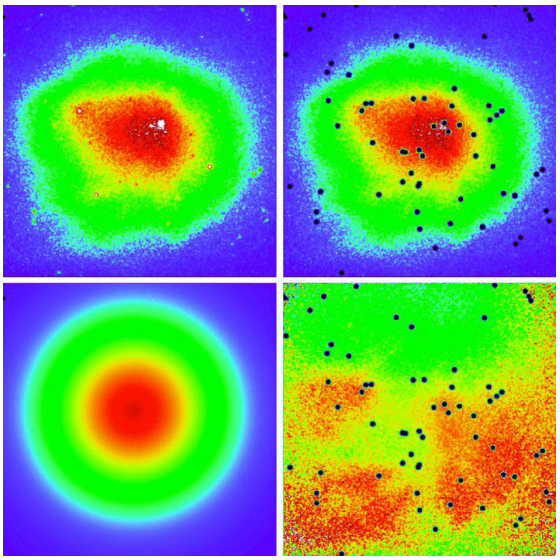

Figure 7. Top Left: XMM image of the Coma cluster. Top Right: The same XMM image with detected X-ray point sources removed. Bottom Left: Azimuthally symmetric beta-model image representing Coma with β = 0.6 and r_{core}=245 kpc. Bottom Right: Residual image of Coma after dividing by the β-model image, illustrating modest fluctuations in the surface brightness of the intracluster medium (Churazov et al. 2012).

viations, and estimated the volume-filling fraction of the density fluctuations of the ICM relative to a smooth, continuous distribution on physical scales of 30–500 kpc. There was remarkably little variation in these fractions, ranging from 7–10% on scales of 500 kpc to 5% on 30 kpc scales. Churazov et al. (2012) were able to place testable constraints on the importance of perturbations in the gravitational potential by constituent galaxies in Coma, as well as the relevance of turbulence and entropy variations. Sanders & Fabian (2012) performed a similar study with XMM and Chandra observations of the much cooler, but more relaxed cluster AWM 7 and found similar density fluctuations, indicating that on small (~30 kpc) scales, cluster physics (e.g., conduction and viscosity) is similar for both high mass and low mass clusters.

XMM continues to play a vital role in confirming candidate clusters of galaxies detected via the Sunyaev-Zeldovich effect with Planck. The Planck Collaboration et al. (2011a-d) has completed a number of highly cited studies whose results are heavily reliant on XMM observations to establish which Planck candidates are bonafide clusters. In addition to confirming 51 new clusters (The Planck Collaboration et al. 2013a), the combination of XMM and Planck coupled with lensing mass estimates of clusters is placing useful constraints on cluster gas pressure, gas and total masses, and baryon fractions in the outer, virialized regions of clusters (The Planck Collaboration et al. 2013b).

Future Cluster Research

Using X-ray clusters as cosmological tools continues to be one of XMM's major contributions to astrophysics. Future research is focusing on observing X-ray cluster emission beyond r_{500}, where the gas density, pressure, entropy, mass, and baryon fraction provide increasingly more leverage in distinguishing among competing cosmological models. The large collecting area of XMM provides the ability to collect the requisite photons needed to study these low surface brightness outer regions. The validation of Planck-detected cluster candidates also remains a key area for which XMM can significantly advance cluster research. While Planck is expected to detect over 2000 bonafide clusters, it will also identify an unknown number of false detections due to fluctuations in the complex microwave sky. Detecting the X-ray emission from a bonafide, mature cluster is therefore crucial for constructing an unbiased cluster sample. With its large collecting area, even a snapshot XMM observation can detect any Planck-detected cluster to a redshift of z ≤ 1.5. Recent large programs accepted by XMM are building volume-limited samples of clusters to further constrain cosmological parameters, determining the chemical enrichment in clusters and groups, determining the dark matter distributions in high redshift clusters, and getting spectra of the Sculptor Wall to determine if it is WHIM-like gas or a galactic halo. Several of the XMM surveys (e.g., the XXL survey) will detect many new clusters and groups.

The high spectral resolution of the RGS enables the measurement of the velocity broadening of intracluster or intragroup gas due to cosmologically induced turbulence, AGN feedback, or sloshing of gas within the cluster or group potential well. Sanders & Fabian (2013) used RGS data to detect velocity broadening on the order of 400 km s^{-1} in a cluster (Abell 3112), two groups (HCG 62 and Fornax), and an elliptical galaxy (NGC 4636), while only finding upper limits of ≤ 300 km s^{-1} in several other targets. This implies that turbulence, AGN feedback, and sloshing must play a variable role in different clusters/groups/galaxies, and bears further investigation.

1.4.3 Galaxies

Elliptical Galaxies: Once thought to be "simple" systems, ellipticals have shown themselves to be very complex objects. The diffuse hot plasma is due to stellar mass loss, SNIa, and perhaps accretion,

and thus provides sensitive tests of models of the gas production, loss, and accretion, as well as a means of tracing the total mass distribution. From the current stellar abundances one would expect the ISM to have strongly super solar abundances, yet observations find sub-solar (X-ray faint ellipticals) to roughly solar (X-ray bright ellipticals) abundances. An extensive set of physical mechanisms and observational biases have been proposed to ameliorate the abundance problem. XMM routinely detects diffuse emission to large radii, enabling the largest possible lever arm with which to determine the baryon fraction (often near cosmic values) and the abundance profile.

Su & Irwin (2013) use XMM data from 32 galaxies, spanning a range of optical to X-ray ratios and environments, to show that Fe abundances are not as low as previously thought, though there is still no correlation between gas and stellar abundances, and no correlation with the amount of neutral gas (though there may be an anti-correlation between Fe abundance and the ratio of molecular gas mass to the hot gas mass). In contrast to this large-scale statistical sample, Humphrey et al. (2012) and Loewenstein & Davis (2012) are, galaxy by galaxy, building small samples of extensively studied galaxies. The latter studied the bright Virgo elliptical NGC 4649 with the RGS in order to measure a broad range of elements. Using the abundance ratios, they show that significant low-metallicity infall is required, even when the SNIa rate is decreased.

Humphrey et al. (2012) studied the faint isolated elliptical NGC 1521. Their analysis concentrated on probing the mass distribution, confirming that this galaxy has dark matter halo consistent with lambda cold dark matter (ΛCDM), and a total mass profile with a power law form. They suggest that this result confirms that the dark matter fraction within the optical effective radius sets the tilt of the fundamental plane.

The XMM RGS has also allowed de Plaa et al. (2012) to place limits on the turbulent velocities in two ellipticals by measuring the resonant scattering in the Fe XVII 15.01 Å and 17.05 Å lines. Although this analysis is made uncertain by the limits in the atomic data, it demonstrates the potential of the RGS to constrain models for the turbulence in the ISM of ellipticals and to provide further clues about their merger histories.

Spiral Galaxies and their Halos: One of the prime questions concerning spiral galaxies is the location and composition of the "missing baryons." It has been assumed that many of the missing baryons are in the form of a hot halo. The difficulty in determining the scale of the Galaxy's hot halo, and the difficulty in detecting halos around other spiral galaxies left this question unsettled. Finally, following a similar detection in NGC 1961, Dai et al. (2012), observing the fastest rotating spiral, UGC 12591, show that the hot halo contains only ~30% of the baryons expected. Given a similar result for the Milky Way (Miller & Bregman 2013, see below), XMM observations strongly indicate that missing baryons are not in hot galactic halos.

Even if halos do not contain the keys to the missing baryon problem, they are interesting in themselves. Halos can be formed by either infall or galactic fountains, and it is not clear which mechanism dominates. Thus, halos may either contain a large amount of low-metallicity material (essential for most chemosynthesis models), or record the star-formation history in enriched material. Starburst galaxies are expected to represent the metal-rich extreme, but even here the evidence is equivocal. XMM observations by Hodges-Kluck & Bregman (2013) of the edge-on NGC 891 reveals either a low-metallicity single temperature component spectrum or a solar metallicity two-temperature component spectrum. On the basis of cooling rate and scale height arguments, they favor the low metallicity case, but the results are not conclusive. Conversely, Mitsuishi et al. (2013) studying NGC 253 with a combination of XMM and Suzaku found the halo to have the same α-enhanced abundances as the superwind.

Dark Matter in Galaxies: XMM's large effective area has allowed it to be used to search for narrow emission lines from radiatively decaying dark matter, in particular those from the sterile neutrino. Borriello et al. (2012) searched for such emission from the core of M33 without success. Loewenstein & Kusenko (2012) searched the dark matter rich, X-ray faint, dwarf spheroidal galaxy Willman I, having detected a possible 2.5 keV line with Chandra. They found no narrow emission lines in the 2–10 keV range, and therefore have placed significant constraints on this dark matter candidate.

Stellar Disruptions in Galaxies: Some X-ray flares may be produced when an otherwise dormant nuclear SMBH tidally disrupts a star. These tidal disruption events have become more important in this era of large-scale temporal surveys and remain poorly understood. Several candidate events have been identified, but catching such events near their peak is difficult. However, Saxton et al. (2012) have demonstrated that monitoring the XMM slews, since they cover a large area, can detect bright candidate disruption events, finding one in SDSS J120136.02+300305.5, a seemingly normal galaxy not containing an AGN. As in the case of the Swift-detected candidate J1644+57 with a possible QPO

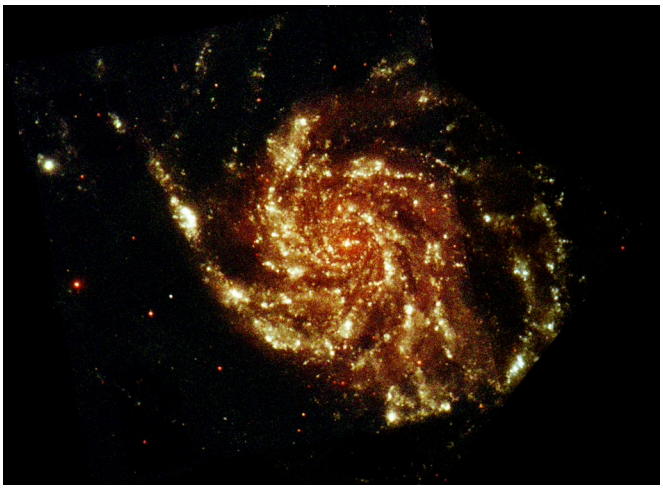

Figure 8. XMM OM UV image of the Pinwheel galaxy M101 (red=2000–4000 Å, green=2000–3000 Å, and blue=1750–2750 Å), illustrating the potential of the OM data to determine stellar populations in galaxies (Miller et al. 2012). The same data were used as part of a survey that showed that ~90% of ULXs are located in young star forming regions (Berghea et al. 2013).

(Reis et al. 2012), XMM pointed observational follow-up was required to characterize the spectrum and short-term variability, as well as to follow the events as they faded over several orders of magnitude. There are currently too few of these events to draw broad conclusions; XMM will remain a key instrument for further study.

Charge Exchange Emission in Galaxies: Charge exchange emission may arise from interfaces between hot X-ray emitting plasmas and cool, neutral gas. Intermediate warm ionized regions may "insulate" the neutral gas from the hot plasma sufficiently to prevent charge exchange. Liu et al. (2011) claim to find charge exchange emission in the He-like oxygen triplet in RGS spectra of the center of M82, while Ranalli (2012) makes a similar claim for NGC 5236. Liu et al. (2012), using the RGS, find evidence of charge exchange in the spectra of the nuclei of several nearby galaxies. In all cases, the claim is based on the triplet ratios being similar to that of a purely recombining plasma, rather than one in collisional ionization equilibrium (CIE). Since this diagnostic does not distinguish between charge exchange and recombination, the true emission mechanism remains unclear. Although Astro-H will have the high spectral resolution to attack this problem, the spatial resolution is poor, which may significantly dilute the charge-exchange signal. Thus, the RGS will continue to play a crucial role in understanding whether charge exchange emission arises from the interstellar medium (ISM) in galaxies.

UV Observations of Galaxies: XMM's contribution to galactic science is not limited to X-rays. The Optical Monitor, providing optical and UV coverage, has been shown to be a useful tool for galaxy evolution studies in clusters (Fig. 8; Miller et al. 2012), though its potential has not been fully explored!

1.4.4 Diffuse X-rays from the Milky Way and Solar System

Diffuse X-rays from the Galactic Halo, Galactic Disk, and the Solar Neighborhood: The hot Galactic halo has long held the possibility of containing the missing baryons within the Galaxy; the difficulty in determining the distance to the emitting plasma, and poor constraints on its metallicity, have stymied efforts to resolve the missing baryon problem. Miller & Bregman (2013), using high-resolution RGS spectra of the OVII line from 29 lines of sight through the Milky Way halo and bulge, have placed strong constraints on the shape, size, and density of the halo. They find that the hot plasma contains between 10 and 50% of the missing baryons in the Milky Way under reasonable assumptions about the metallicity. Their results are surprisingly robust with respect to the uncertainty in the metallicity, and are consistent with a broad range of external constraints, from emission measures to high velocity cloud pressures.

Diffuse X-ray emission from the halo of the Milky Way, the disk, and the Local Hot Bubble fill the entire FOV. Given XMM's large FOV, strong soft response, and well-characterized instrumental backgrounds, XMM is the best operating mission for studies of diffuse emission. Recent progress has been complicated by solar wind charge exchange (SWCX) emission, a time-variable foreground component whose spectrum and spatial distribution are poorly characterized. (Absorption-line studies are mercifully free of this complication.) Thus, studies of diffuse Galactic emission usually require simultaneous study of the SWCX emission. Henley & Shelton (2013, 2012) extracted the background spectra from all available MOS observations to characterize the distribution of OVII and OVIII emission lines due to the halo, the disk, and the SWCX. After careful data selection to minimize the SWCX component, they found that the Galactic halo spectrum has a relatively uniform mean temperature (2.2×10^6 K) but a patchy distribution of emission measure.

The SWCX emission arises both from the near-Earth environment (in the magnetosheath) and throughout the heliosphere. Specialized, highly constrained observing strategies are being used (Snowden et al. 2009, and further observations executed in December 2013) to test rigorously the extensive hydrodynamic models of the magnetospheric component of SWCX (Siebeck et al. 2014). These observations will also constrain the charge exchange

Future Solar System Research

In the coming cycle there will be a multi-spacecraft, multi-wavelength campaign, including XMM, to study the auroral X-ray emission from Jupiter. Due to its strong magnetic field, the origin of energetic particles can be determined by the location of their impact with the Jovian atmosphere; hard X-rays coincident with the far ultraviolet (FUV) aurorae are due to particles originating in the Io plasma torus, while soft X-rays originate further out, possibly in the solar wind itself (Branduardi-Raymont et al. 2007). By correlating the X-ray emission, FUV auroral emission, and solar wind parameters, energetic particle sources and production mechanisms will be determined. These types of observations of planets in the Solar System, for which XMM is well suited, are laying the groundwork for X-ray observations of extra-solar planets with future missions. See Koutroumpa et al. (2012) for a discussion of these exciting possibilities.

cross-section for O^{+7} and O^{+8} with H, which can then be used to constrain the heliospheric emission.

Solar System Studies: Charge exchange emission due to the solar wind has now been detected from the Earth, Venus, Mars, Jupiter, Saturn, and numerous comets. For many of these objects, there are multiple sources of X-ray emission, including fluorescence and scattering of solar X-rays. XMM's large collecting area and strong soft X-ray response is well suited to the study of this emission, while the RGS is essential for the spectroscopic determination of the relative emission from the different processes.

Since Mars has no magnetic field, the solar wind interacts directly with the extended outer Martian atmosphere, producing charge-exchange emission, while the inner Martian atmosphere fluoresces and scatters X-rays. Multiple observations of Mars with different instruments have produced very different results, in part because of the solar cycle. The recent sophisticated modeling by Koutroumpa et al. (2012) matches the observed spectro-spatial distribution quite well, but is unable to match the intensity of the XMM observations taken during solar maximum. This discrepancy may be due to peculiar solar wind conditions during the observations; further observations over the next few years, also during solar maximum, will resolve this situation.

1.4.5 Stars and Star Formation

Studies of stars, star and planet formation, and stellar evolution in the Milky Way continue to exploit three of XMM's main capabilities: imaging spectroscopy of star-forming regions and OB associations (large FOV and good spatial resolution of EPIC), imaging spectroscopy of individual X-ray sources (large effective area of EPIC), and grating spectroscopy of bright sources (large effective area of the RGS from 6–40 Å).

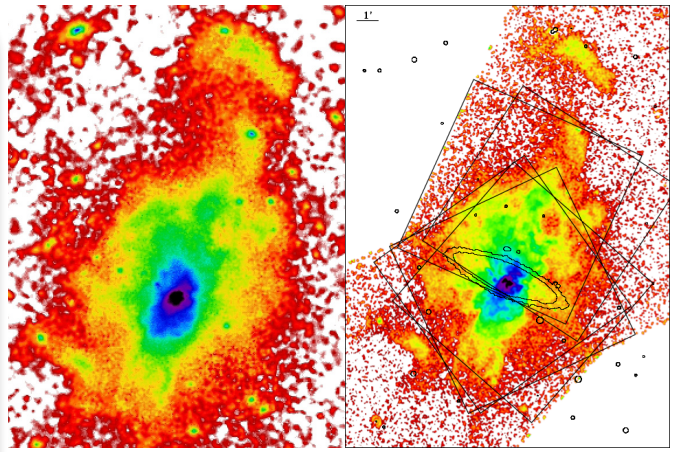

Figure 9. Two views of M82, one from XMM (left) showing a mosaic of ~130 ks of cleaned data in the 0.4-1.3 keV band and one from Chandra (right) showing a mosaic of 466 ks of data. The boxes note the location of the S3 chip, which has a soft response comparable to that of the XMM instruments. The regions outside those boxes were observed with the S2 and S4 chips that have much poorer soft response. The XMM image clearly shows extended soft diffuse emission at much fainter levels than Chandra over a much more extended region.

Star-Forming Regions: XMM observations of Galactic star-forming regions continue to identify interesting new X-ray sources. Star-forming regions are ideal targets for XMM EPIC because they contain hundreds to thousands of coeval young stars spanning the entire initial mass function. Pillitteri et al. (2013b) and Fang et al. (2013) used the Survey of Orion with XMM and Spitzer (SOXS) survey of the Orion A cloud to detect cluster members and identify sub-clusters around the L1641 dark cloud and the O9 giant ι Orionis.

Mernier & Rauw (2013) used a set of EPIC observations of the M17 (Omega Nebula) region to show that the three brightest massive stars are most likely colliding wind binaries, while the million-year-old pre-main-sequence (PMS) stars show significant long-term X-ray variability. Pires et al. (2012) discovered the isolated neutron star 2XMM J104608.7-594306 in the Carina nebula.

Massive Stars: The brightest stellar X-ray sources are the massive luminous blue variables (LBVs), Wolf-Rayet stars, and OB stars, whose X-ray emission is connected to their strong winds, producing embedded wind shocks, colliding wind shocks (for the massive binaries), and magnetic wind shocks (for the magnetic massive stars). The LBV η Carina has been observed nearly every year by XMM since its launch in 1999. Extensive 3D simulations of the wind

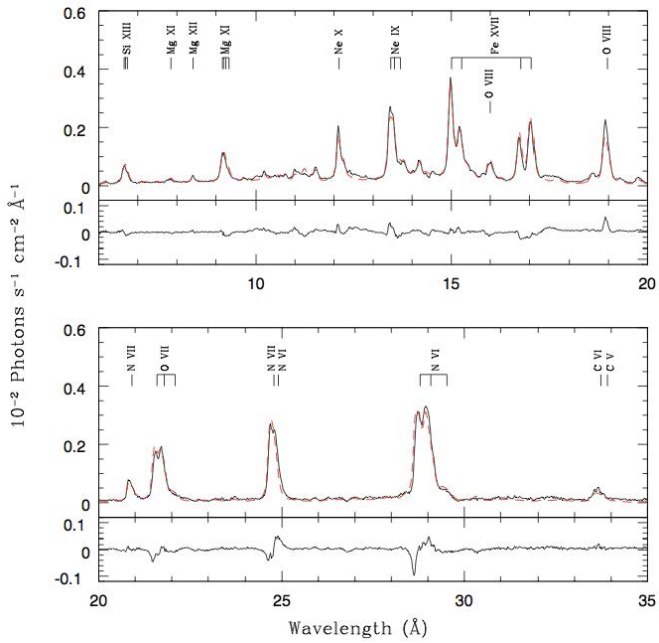

Figure 10. Upper Panels: Best-fit model (dashed red line; Hervé et al. 2013) of the 1 Ms 5–20 and 20–35 Å RGS spectra of ζ Pup (solid black line). Lower Panels: Observed minus model residuals. The most prominent emission lines are labeled.

collision between the LBV η Car A and its massive companion η Car B suggest that the mass-loss rate of the LBV dropped by a factor of 2–3 between 1999 and 2010 (Madura et al. 2013; Russell et al. 2013). The large effective area of the EPIC cameras is ideal for obtaining medium-resolution X-ray spectra at high time cadence of X-ray bright stars like η Car.

Motivated by the expanding archive of RGS and Chandra HETG spectra, several groups have developed detailed emission/absorption models of hot star wind shocks embedded in a clumpy wind (e.g., Hervé et al. 2012; Sundqvist et al. 2012; Leutenegger et al. 2013). Hervé et al. (2013) and Nazé et al. (2013) used the 1 Ms XMM data set of the prototypical early-O supergiant ζ Puppis (Fig. 10) to identify a slow (many days) modulation of its X-rays, possibly as a result of corotating interaction regions. More surprising perhaps was the lack of significant short-term variability (<1%), showing that the wind is highly fragmented. Their embedded wind shock emission/absorption model requires >10^5 wind clumps.

Using high signal-to-noise XMM RGS and Chandra HETG line profiles, Leutenegger et al. (2013) found that individual clumps in the wind are not optically thick, implying low wind porosity. Taken together, the two sets of results have led to a fundamental advance in our understanding of massive star winds: (i) mass-loss rates are a factor of 2–3 lower than predicted by unclumped wind models, and (ii) the winds are made up of hundreds of thousands of relatively small clumps that shock to emit X-rays.

Ground-based optical spectropolarimetry of OB stars has been used to show that ~10% of massive stars possess large-scale, fossil magnetic fields (Wade et al. 2013). These stars may be the precursors of highly magnetic neutron stars. In the presence of magnetic fields, massive-star winds are channeled and confined, producing X-ray emitting shocks (Oskinova et al. 2011; Gagné et al. 2011). Petit et al. (2013) compiled a comprehensive set of inferred and observed stellar and magnetic parameters of OB stars to construct the first magnetic confinement vs. rotation classification of massive-star magnetospheres.

T Tauri Stars: The PMS T Tauri stars have X-ray activity levels that are 10^3–10^4 higher than older late-type stars like the Sun. Though some of this may be scaled up dynamo-driven coronal activity, X-ray spectroscopy of accreting, classical T Tauri stars (CTTS) now suggest that the X-rays are produced in high-density accretion shocks. Günther et al. (2013) use XMM and Very Large Telescope (VLT) Ultraviolet and Visual Echelle Spectrograph (UVES) observations of the T-Tauri star MN Lup to determine its shock density and accretion rate. MN Lup is unusual because it shows clear signs of accretion, but no dust disk, suggesting it may be in a short-lived phase of gas accretion after its disk has dissipated.

The young binary AK Sco consists of two F5 PMS stars in a small, highly eccentric orbit. Separated by only 11R_* at periastron, Gómez de Castro et al. (2013) find X-ray and UV fluxes enhanced by a factor of three during periastron passage. The XMM and HST data suggest that, "the eccentric orbit acts like a gravitational piston. At apastron, matter is dragged efficiently from the inner disk border, filling the inner gap and producing accretion streams that end as ring-like structures around each component of the system. At periastron, the ring-like structures come into contact, leading to angular momentum loss, and thus producing an accretion outburst."

Extrasolar Planets: The explosion in the number and variety of exoplanets in recent years has prompted a variety of studies on the viability of exoplanet atmospheres around stars spanning a wide range of masses and activity levels, from very low-mass dMe stars and brown dwarfs, G- and K-type dwarfs, and intermediate-mass T-Tauri stars.

Recent studies have focused on possible star-planet interactions: the interaction of the planetary atmosphere/magnetosphere with the magnetosphere/corona of the host star (Cohen et al. 2011; Poppenhaeger et al. 2013; Stark et al. 2013). Pillitteri et al. (2011) used the rotational phase of two XMM flares on HD 189733 to suggest an interaction between planet and stellar magnetic fields when the

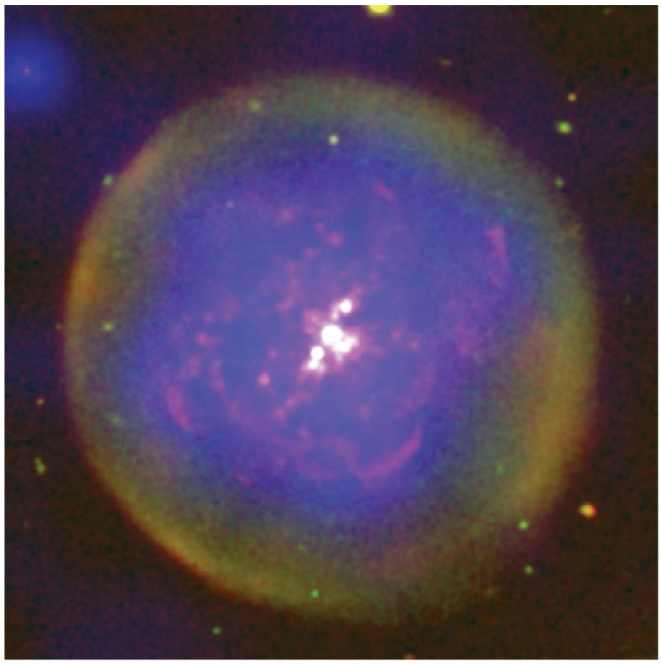

Figure 11. Comparison of ground-based, narrow-band optical and XMM images of the born-again planetary nebula A30 (Guerrero et al. 2012), showing the large-scale spatial distribution of O III (red), Hα (green) and 0.19–0.60 keV X-ray emission (blue; Guerrero et al. 2012).

planet passes close to active regions. The RGS spectra were used to show that the active regions on HD 189733 are unusually dense.

The XMM spectra and light curves of two other hot Jupiter systems were more controversial. HD 162020 showed only marginal orbital modulation, while WASP-18, a 600-Myr old F6 dwarf, is X-ray dark (Pillitteri et al. 2013a), suggesting that the hot Jupiter may have disrupted the convection zone of the star, thereby quenching its corona.

Further XMM monitoring data are needed to assess (i) the prevalence of star-planet interactions, (ii) the impact of high-energy irradiation on exoplanetary atmospheres, and (iii) the role of the interactions on the magnetic fields and angular momentum evolution of the star-planet system.

Planetary Nebulae: XMM imaging spectroscopy combined with ground- and space-based optical spectroscopy of planetary nebulae have yielded important insights into the mass-loss histories of their progenitors. For the Wolf-Rayet and PG1159-type central stars of planetary nebulae, it appears that they were "born again": a late helium shell flash dredged up carbon-rich material, ejecting it into the circumstellar environment.

Guerrero et al. (2012) used XMM and Chandra imaging spectroscopy of the born-again planetary nebula A30 to identify a central point source, and diffuse emission associated with the hydrogen-poor knots and the lobed bubble inside the nebular shell (Fig. 11). Multi-epoch HST images were used to derive an expansion age of 850 yr. The combined data suggest that the diffuse X-rays are generated by the post-born-again and present fast stellar winds interacting with the hydrogen-poor ejecta of the born-again event. Similarly, serendipitous X-ray detections of the PG1159-type central star of the planetary nebula K 1-16 show carbon-rich, 10^6 K optically thin emission, providing further support for the born again scenario (Montez & Kastner 2013).

1.4.6 Supernova Remnants (SNRs)

Galactic SNRs: The soft band sensitivity and large field of view of XMM makes it a powerful tool for the study of SNRs in our Galaxy and beyond. Galactic SNRs provide detailed studies of shock and particle acceleration physics, as well as the evolution of and associations with pulsars and other compact stellar remnants. Since the last SR, observations from XMM have been at the forefront of discoveries in these areas of SNR research, such as the discovery of a pulsar wind nebula candidate in the Cygnus Loop (Katsuda et al. 2012b). This candidate is far off center, suggesting a very high kick velocity (~1850 km s^{-1}) if confirmed.

Over the past few years, XMM observations of Galactic SNRs have proven essential to some fundamental discoveries concerning shock physics. For example, the spectral resolution and soft sensitivity allowed spatially resolved X-ray spectroscopy of SN 1006, which shows high post-shock compression ratios supporting acceleration of cosmic ray hadrons in post-shock plasma in SNRs (Miceli et al. 2012). Furthermore, XMM data allowed detailed pulsar wind nebula modeling of G0.9+0.1 (Holler et al. 2012), where the X-ray data are well fit with a leptonic outflow that loses energy to adiabatic expansion and synchrotron interactions. These models are still highly uncertain, and results from different groups can disagree by orders of magnitude. These data provide some of the best constraints available for modeling these complex particle acceleration processes.

The spectroscopic capabilities of XMM make it even more powerful for Galactic SNRs, as they are bright enough for grating spectroscopy with the RGS. For example, high-resolution X-ray spectroscopy from XMM has led to the detection of charge-exchange emission in Puppis A (Katsuda et al. 2012a). This emission comes from the interaction of highly ionized and neutral particles where the shock-heated gas touches clouds in the ISM. Charge exchange X-ray emission in SNRs had been theoretically suggested since the 1970s, but had not been detected in Puppis A until last year. Another recent example is the direct measure of ejecta temperatures and ve-

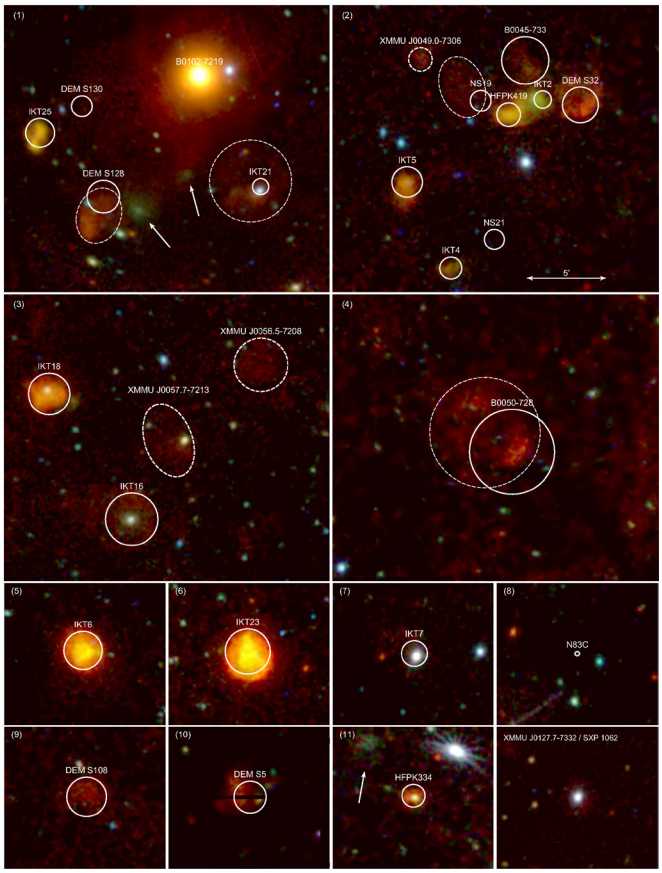

Figure 12. Supernova remnants in the SMC as seen by XMM EPIC. The RGB color image is composed of the three energy bands 0.2–1.0 keV (red), 1.0–2.0 keV (green), and 2.0–4.5 keV (blue) (Haberl et al. 2012).

locities in Puppis A with RGS spectroscopy (Katsuda et al. 2013).

Extragalactic SNRs: The high sensitivity of XMM makes it of excellent use for studies of extragalactic SNRs. In the Magellanic Clouds, XMM can resolve the structure of SNRs. Outside of the Galactic satellites, even though XMM is not capable of resolving the SNR structures, it can detect and constrain the spectra of SNRs with less observing time than other missions. Just measuring X-ray fluxes for these objects can provide critical support for their identification (SNRs or H II regions) and physical state (energetics).

The soft sensitivity of XMM has resulted in a remarkable efficiency for detecting faint extragalactic SNRs. For example, XMM observations have led to the discovery of a new SNR in the LMC (Grondin et al. 2012), and has confirmed several SNRs in M31 (Sasaki et al. 2012). The diffuse emission from the superbubble N206 was reliably characterized and the energy associated with the hot gas determined with just 50 ks of data in the MOS camera. While most of the hot gas was clearly shock-heated and contained within the Hα shell, the XMM data also showed faint hot gas outside the Hα shell (Kavanagh et al. 2012), indicating that shock-heated gas had escaped into the surrounding ISM.

Future Studies of Galactic SNRs

The wide field of XMM will be used to map the structure of large Galactic SNRs. For example, such a program was approved as a large program for AO-12. A US-led (PI: Smith; Program: 072163) large program (300 ks) will map the Galactic SNR W44. They will model the ionization structure and state of the plasma with 3-dimensional magnetohydrodynamic simulations to study the connection between such highly ionized SNRs and triggered star formation.

XMM's large FOV makes it a valuable resource for extragalactic SNR studies. An excellent example is the survey of the entire Small Magellanic Cloud (Haberl et al. 2012) that is the deepest survey of any entire galaxy in X-rays to date. The extensive areal coverage (several deg^2) and a sample of SNRs are shown in Fig. 12. This survey has found 4 new SNRs (Maggi et al. 2013), along with providing the most detailed X-ray images and spectra for dozens of previously known SNRs. The science output from this survey has only begun.

The excellent spectral resolution of XMM enables the study of details of shock physics in extragalactic SNRs. Recently, spectra from XMM have provided new and exciting constraints on models of the interaction of SN1987A with its surrounding HII region (Dewey et al. 2012) from its broad X-ray line emission. Further, XMM observations put the tightest constraints on the continually evolving lightcurve of 1987A (Maggi et al. 2012). These observations are allowing us to watch a SNR form and evolve from birth, observing the luminosity grow as the SNR sweeps up interstellar matter into the shock front.

1.4.7 Neutron Stars (NSs)

NSs are laboratories for the study of matter at densities higher than nuclear, while their populations are a tracer of massive star formation and a window into the physics of supernova explosions. The high-throughput imaging and timing simultaneously available with the XMM EPIC cameras are needed to determine the physical properties of the majority of isolated pulsars that are radiatively inefficient at all wavelengths, and are often detectable only in X-rays. X-ray measured spin-down rates determine the pulsars' ages, dipole magnetic field strengths, and spin-down luminosity.

"Ordinary" Pulsars: Interesting new phenomenology has been discovered by XMM observations of isolated NSs. For the first time, a change of X-ray

properties in a rotation-powered pulsar has been observed, in conjunction with the phenomenon of mode-switching in the radio (Hermsen et al. 2013; Mereghetti et al. 2013). The emission from PSR B0943+10 switches from unpulsed to pulsed, and the X-ray flux increases by a factor of 2.5, in concert with the radio state transition. Previously, rotation-powered pulsars all had very stable X-ray properties. This new behavior points to a global change in the pulsar magnetosphere and is yet to be well explained by any model.

A pulsar with possibly the highest kick velocity, PSR J1101-6101, was recently discovered by Tomsick et al. (in preparation) in an AO-12 XMM observation of the INTEGRAL source IGR J11014-6103. This 62.8 ms pulsar has a bow-shock in X-rays that points away from the SNR MSH 11-61A, and requires a velocity >2400 km s^{-1} to have originated in that remnant, given its distance and age. XMM has discovered several extremely long X-ray tails of uncertain origin from pulsars, including a second feature from PSR J1101-6101 that is perpendicular to its bow shock, and one from the middle-aged Fermi pulsar PSR J0357+3205 that is a record 9′ long, and possibly of bremsstrahlung origin (Marelli et al. 2013).

Using timing observations, Halpern et al. (2013) established that the 44 ms PSR J1813-1749, which powers the TeV emission from HESS J1813-178, and is also an INTEGRAL source, is the second most energetic rotation-powered pulsar in the Galaxy, with a spin-down luminosity of 5.6 x 10^{37} erg s^{-1}. Many such energetic pulsars are radiatively inefficient, and not detected in radio, nor by Fermi, but are waiting to be discovered and timed in X-rays.

Millisecond Pulsars (MSPs): The year 2013 was a milestone in the study of the evolution of MSPs. These rapidly spinning NSs are theorized to originate in LMXB, where they are spun up (recycled) to millisecond periods by accretion, and emerge as rotation-powered, radio MSPs when the accretion stops. For the first time, switching between rotation-powered and accretion-powered states has been observed in a pulsar system, supplying the missing link between the radio MSPs and their LMXB progenitors, and providing strong support for the recycling theory. In March 2013, the INTEGRAL satellite detected a bright transient source IGR J18245-2452 in the globular cluster M28. Follow-up observations with XMM (Papitto et al. 2013) using the EPIC pn CCD in timing mode discovered X-ray pulsations with a period of 3.93 ms and an orbit of 11 hr (Fig. 13), exactly matching the timing parameters of PSR J1824-2452I, a previously known radio pulsar in the cluster, and proving that the transient LXMB and the radio MSP were the same object. When accreting

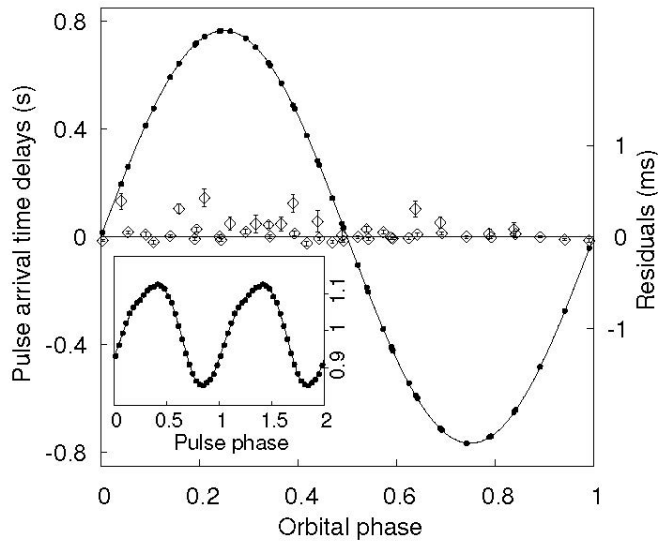

Figure 13. X-ray pulse profile (inset panel, 3.93 ms spin period) and 11 hr orbital period modulation of the transition MSP/LMXB IGR J18245-2452/PSR J1824-2452I during its X-ray outburst, using the EPIC pn CCD in timing mode (Papitto et al. 2013).

material penetrates within the light cylinder of the radio pulsar and falls onto the polar caps, it quenches the radio pulsation mechanism and replaces it with X-ray pulsations.

In June 2013, radio pulsations from another binary MSP, the 1.69 ms PSR J1023+0038, were observed to turn off for the first time since their detection in 2007, indicating that it has probably started accreting. There had been evidence that this 4.8 hr binary was accreting in 2000-2001, when optical emission lines and the blue continuum characteristic of an accretion disk were seen. Now accretion has resumed, as evidenced by enhanced optical and X-ray emission observed after the radio pulsations turned off. With a flux of 1 x 10^{-11} erg cm^{-2} s^{-1}, the 0.3–10 keV X-rays from PSR J1023+0038 were not quite bright enough to trigger any all-sky monitor, but an entire XMM revolution was used to observe it in October 2013 (PI: Bogdanov). This observation will enable X-ray pulsations to be detected, if they are present, as in PSR J1824-2452I. Variable emission from the accretion disk, and orbital modulation in the optical due to heating of the illuminated face of the companion star will also be studied. PSR J1023+0038 was previously observed by XMM in its quiescent radio pulsar state (Archibald et al. 2010), which revealed X-ray emission modulated on the orbital period with a maximum at superior conjunction of the companion star, demonstrating the existence of the predicted intrabinary shock between the pulsar wind and the ablated face of the companion. Now an accretion disk has formed, which is fighting the pressure of the pulsar wind close to the NS.

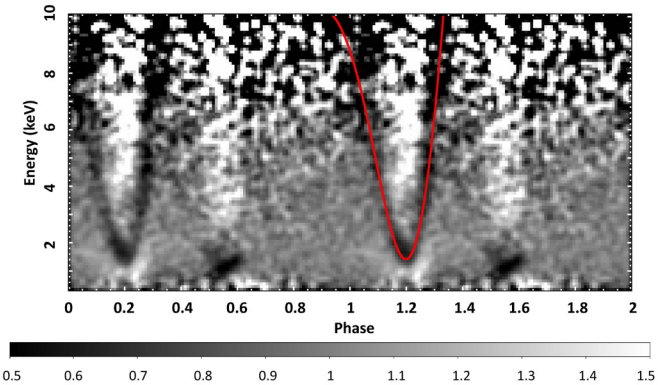

Figure 14. Phase-dependent spectral feature in the XMM observation of the magnetar SGR 0418+5729 (Tiengo et al. 2013). A normalized image of energy versus rotation phase was constructed by binning the EPIC source counts into 100 phase bins and 100-eV-wide energy channels. The red line shows the results of a simple proton cyclotron model consisting of a baryon-loaded plasma loop emerging from the surface of the magnetar.

This is evident from rapid X-ray fluctuations, and enhanced Fermi gamma-ray flux coming from a now more luminous shock.

Both PSR J1023+0038 and IGR J18245-2452 are nearly Roche-lobe-filling systems called "redbacks," which are related to the black-widow pulsars, the energetic MSPs that have nearly evaporated their companion stars. These and other eclipsing millisecond pulsars that were once rare are being found in large numbers by Fermi, and are the subject of detailed X-ray study by XMM (e.g., Bogdanov et al. 2013). With its long orbit, 30 μs timing, and high throughput, XMM is uniquely suited to studying the rich X-ray behavior of these complex systems, which display rapid variability while in the accreting state. The OM enables complete coverage of binary orbits, which is often not possible from the ground because of seasonal restrictions and Earth's rotation.

Magnetars and Anti-Magnetars: XMM continues to contribute to the spectral and timing studies of new, outbursting magnetars, especially ones that are faint in quiescence. In recent years, it has become apparent that the majority of magnetars are transient, possibly spending more and more time in a quiescent state as they age, so that we only get to see the older ones only once. Overlap in magnetic field strength has been found between some transient magnetars and ordinary, high B-field radio pulsars, supporting the long-sought unification of NS classes. Spin-down measurements of three transient magnetars indicate dipole fields that are less than the quantum critical value of 4.4×10^{13} G that is traditionally associated with the magnetar class. These are SGR 1822-1606 with $B = 2.7 \times 10^{13}$ G (Rea et al. 2012), SGR 0418+5729 with $B = 6 \times 10^{12}$ G (Rea et al. 2013a), and 3XMM J1852+0033, which was discovered recently in archival data (Fig. 15; Zhou et al. 2013), and has only an upper limit of $B < 4 \times 10^{13}$ G (Rea et al. 2013b). It is necessary to monitor these for months or years to measure their small B-fields, which is only possible using the sensitivity of XMM once they have faded.

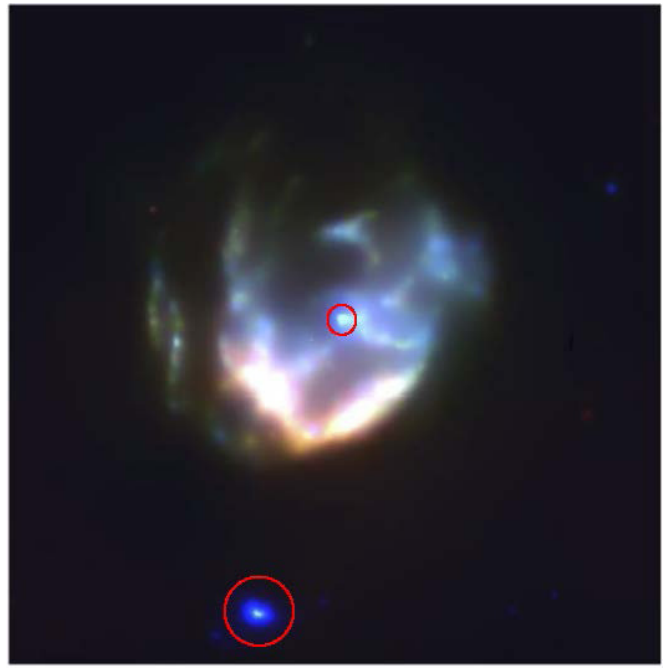

Figure 15. XMM image of a supernova remnant, showing a newly discovered magnetar just outside the remnant (circle at bottom), and a previously known anti-magnetar (circle at center of SNR; Zhou et al. 2013). The colors show the X-ray hardness (red is soft, blue is hard)..

Much evidence for an inherent complexity of magnetic field structure in NSs has come to light in recent years. An analysis of high signal-to-noise, pulse-phase-resolved XMM spectra of SGR 0418+5729 obtained soon after its outburst revealed a remarkable absorption line, shifting between 1 and 10 keV in a narrow interval of rotation phase (Fig. 14, Tiengo et al. 2013). Because this energy is much smaller than the expected electron cyclotron resonance at 70 keV for the dipole field of $B = 6 \times 10^{12}$ G, it was modeled as proton cyclotron scattering from a magnetic loop just above the NS surface, with $B > 2 \times 10^{14}$ G. Such strong field-line bundles are the basis of the twisted magnetosphere model for magnetars, which requires that much stronger fields reside in the crust of the NS than is evident from their spin-down dipole moments.

Even NSs with the smallest magnetic dipoles are likely to have intrinsic magnetic fields that are evolving. The thermally emitting central compact objects (CCOs) in SNRs are more common than magnetars. The "antimagnetar" nature of CCOs was confirmed

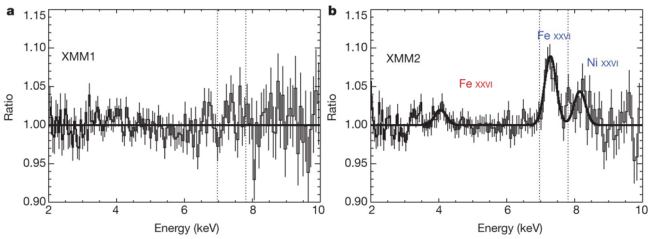

Figure 16: X-ray spectra of the baryon relativistic jet X-ray binary 4U 1630-47 (Diaz Trigo et al. 2013). The figures show residuals from the fitted continuum spectra of 4U 1630-47 in two states: (a) radio off, and (b) radio on. The latter has blueshifted and redshifted emission lines. The dotted vertical lines indicate the rest energy of the transitions of Fe XXVI (6.97 keV) and Ni XXVII (7.74 keV).

by recently concluded timing campaigns with XMM that measured precise spin-down rates for two of them (Gotthelf et al. 2013). These are in Puppis A (B = 2.8 x 10^{10} G), and 1E 1207.4-5209 (B = 9.8 x 10^{10} G). Previously, B = 3.1 x 10^{10} G had been found for the Kes 79 CCO. Because it is difficult to account for their nonuniform surface temperatures without invoking much stronger internal magnetic fields, a leading theory for CCOs posits that they have normal, ~10^{12} G magnetic fields that were initially buried by supernova fall-back debris. These fields will diffuse back out on a time scale of 10^4–10^5 yr, enabling the CCOs to rejoin the ordinary radio pulsar population. Such evolution would account for the missing population of CCO descendants, the "orphaned CCOs," and has the additional benefit of not requiring yet another class of NS to exist that would exacerbate the already apparent excess of NSs with respect to the Galactic supernova rate.

1.4.8 X-ray Binaries

X-ray Binaries in the Milky Way: Until now, the peculiar binary SS 433 was the only object in which baryons are unequivocally seen in relativistic jets, the famous moving Balmer lines with oppositely directed velocities of 0.26c. Recently, an XMM observation of the black-hole candidate 4U 1630-47 (Diaz Trigo, et al. 2013) detected Doppler-shifted emission lines (Fig. 16) that can be identified with Fe XXVI and Ni XXVII from a pair of jets with v=0.66c, and an inclination angle 65° relative to the line of sight. The intensities and widths of the lines restrict the temperature and opening angle of the jets to 21 ± 4 keV and < 4.5°, respectively. The source was caught in the "anomalous accretion state," characterized by a luminous, steep power-law spectrum believed to be from a Compton scattering corona above a standard accretion disk. Simultaneously, radio emission indicative of the recent formation of jets was detected. The authors take this result as evidence that jets can be powered by the accretion disk, from which baryons are expected, and not just by the spin of the black hole, which generates purely leptonic jets with higher Lorentz factors. Because of the high count rate of the source, >1000 s^{-1}, the "burst" mode of the EPIC pn CCD, with its 7 μs time resolution, was needed to prevent pileup and telemetry saturation in this observation.

Future Neutron Star Research

The XMM EPIC pn CCD is the most capable instrument for millisecond timing as well as the most sensitive for the detection of faint X-ray pulsars in general. It will be used to study the energetic, recycled pulsars that continue to be identified in large numbers with Fermi sources. As for young NSs, many of the most energetic ones are radio quiet, including a large fraction of those powering pulsar wind nebulae detected by HESS and INTEGRAL. The high throughput of XMM will enable it to discover and time these pulsars. The faint, quiescent counterparts of new transient magnetars that appear on a yearly basis will be studied by XMM. Extended monitoring periods will be necessary in some cases to measure their dipole magnetic fields. Deep observations of the remaining CCOs will be conducted to search for their pulsations. XMM will be at the forefront of efforts to establish a unified understanding of these diverse pulsar populations.

Ultraluminous X-ray Sources (ULXs) in External Galaxies: Whether ULXs represent accretion onto intermediate-mass black holes, or not, has remained a contentious area of research. With apparent X-ray luminosities that can far exceed the Eddington luminosity of a 10 $M_\odot$ stellar-mass black hole, one natural interpretation for the excessive luminosity is that the accreting object has a mass of hundreds to thousands of solar masses in the most extreme cases. Alternatively, beaming or violations of the Eddington limit might explain most if not all ULXs. The expanded X-ray bandpass afforded by joint XMM/NuSTAR observations of ULXs has the potential to distinguish among these competing models (Harrison et al. 2013). Coordinated XMM and NuSTAR observations of NGC 1313 X-1 (Bachetti et al. 2013) and Circinus ULX5 (Walton et al. 2013) both firmly detected a cutoff above 10 keV in the spectra of these sources; this rules out the possibility that these black holes are in a standard low/hard state, and indicates that both these black holes have masses below 100 $M_\odot$.

The Optical Monitor onboard XMM has also been utilized by Berghea et al. (2013) to study the local environment of 27 nearby ULXs and found that nearly all (24 of 27) were associated with star formation

regions younger than 50 Myr, lending support to the notion that ULXs are some form of high-mass X-ray binary (Fig. 8 above).

1.4.9 Cosmology, Surveys, and Serendipitous Science

The recent results from XMM surveys have continued to enlarge and enhance our understanding of the Universe. XMM's large field of view, large collecting area, wide bandpass and good energy resolution have allowed sensitive detailed results from so-called "blind" surveys (deep observations of selected high galactic latitude fields), as well as results on targeted surveys of selected sources such as star clusters, the Galactic plane, and nearby galaxies (as discussed in previous sections).

The XMM-Newton Slew Survey: In addition to the dedicated surveys, XMM is performing an all-sky X-ray slew survey. This will be the deepest and largest solid angle 2–8 keV survey ever performed (Read et al. 2011). There have been major enhancements to the slew survey in the last 2 years with the ability to perform real time analysis, allowing the rapid follow-up of unusual events and transients. Raw slew data are made publicly available on a web page after 8–12 days, having been processed automatically and compared with the ROSAT All-Sky Survey (RASS). Two recent highlights of that program were the detection of TYC 8380, which proved to be a highly-luminous, RS CVn star (López-Santiago et al. 2012), and the discovery of a tidal disruption event (Saxton et al. 2012, discussed in § 1.4.3 above). The quick follow-up of the slew survey data allowed the accumulation of unique X-ray and optical data resulting in one of the best categorizations of a tidal disruption event ever obtained.

The sixth release of the slew survey covers 65% of the sky to a flux depth of 4 x 10^{-12} erg cm^{-2} s^{-1}, five times deeper than the best previous survey in the 2–12 keV band, and 6 x 10^{-13} in the 0.2–2 keV band, roughly similar to the RASS sensitivity. It has over 2000 sources in the 2–12 keV band and 13,000 sources in the 0.2–2 keV band. Over 70% of the sources have been identified from catalogs and other follow-up work. As shown in Warwick et al. (2012), the slew survey provides the crucial link between the HEAO-1 and RXTE slew surveys and the various X-ray deep fields.

The XMM Serendipitous Source Survey (3XMM): The Serendipitous Source Survey involves the processing of all of the XMM public data (Watson 2012). The 3XMM-DR4 catalog (Fig. 17) has made a major improvement in processing and in the availability of results. It has 7432 observations, 67% at high Galactic latitude. The catalog covers 800 square degrees with 372,048 detected sources. Of these, 170,000 have spectra and light curves. The improvements in astrometry have allowed the vast majority of sources to be positioned to better than 2″. Over 40% of the sources have been observed more than once, allowing a systematic categorization of their X-ray time variability. The future of the 3XMM survey includes the extension to multi-wavelength databases, the development of a time variability database, and (of course) the realization of a new catalog in three years.

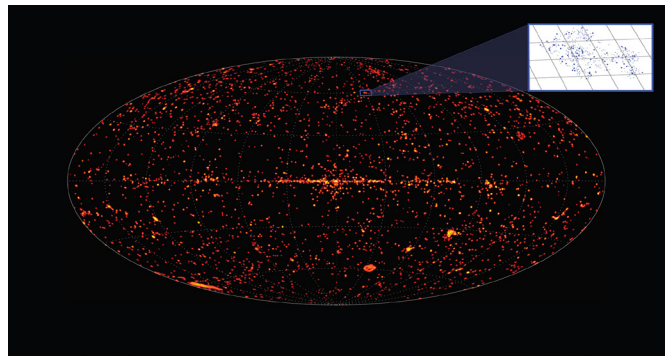

Figure 17. Sky-map of the 3XMM-DR4 Serendipitous Source Survey catalog (Watson 2012). The inset shows a blow-up of a small region of the catalog (decipherable when the electronic version of the proposal is expanded).

Surveys of Nearby Galaxies: Over the last two years, XMM has completed deep, wide surveys of the Large Magellanic Cloud (Haberl 2014) and Small Magellanic Cloud (Haberl et al. 2012; Sturm et al. 2013). In a very surprising result, four new SNRs were detected in the LMC, despite the wealth of multi-wavelength and previous X-ray observations of this nearby galaxy (Maggi et al. 2013, see also § 1.4.6). Three of these four new SNRs have no radio detections. The survey allows the study of iron-rich SNRs, which is not generally possible in the Milky Way due to strong absorption in the Galactic plane. In the SMC, the survey significantly increased the known population of X-ray binaries. The bright-end slope of the luminosity function is considerably steeper than the so-called universal high-mass X-ray binary luminosity function found in nearby massive galaxies, suggesting that a different source population, Be stars rather than LMXBs, dominate in the SMC.

Galactic Plane Survey: The XMM SSC survey of the Galactic plane (Nebot Gómez-Morán et al. 2013) consists of 26 XMM observations obtained at $|b| < 20^{\circ}$, and distributed over a large range in Galactic longitudes. The survey covers a total area of 4 square degrees. It has 1319 sources of which 316 are identified. The identified source population is dominated by active corona stellar sources consisting primarily of a young (100 Myr) to intermediate (600 Myr) age population, with a small contribution of close

main sequence or evolved binaries. The hard band is dominated by extragalactic sources, but there is a small contribution from a hard Galactic population formed by CVs, HMXB candidates, and γ Cas-like systems.

1.5 Summary of Issues

1. Scientific merit

The scientific merit of XMM is extensively detailed in § 1.4. The simultaneous X-ray imaging and spectroscopy coupled with optical/UV observations are unique to XMM, and will remain so. Its wide variety of scientific applications makes it extremely relevant to NASA's Astrophysics research objectives, as noted in § 1.1. The GO program is significantly underfunded, thus able to offer reasonable grants to only ~15 projects per AO (those with US PIs and ranked at the A level). In general, each grant usually supports the analysis leading to both refereed papers and presentations at astronomy/astrophysics meetings. While US PIs with B ranked proposals are allowed to propose for ADAP funding, the success rate is low (one out of six in the last round) leaving researchers without the funds to support their projects.

2. Promise of future impact and productivity

As noted in § 1.4, the LP/VLP programs give a hint as to what may be expected from the current year planning cycle. XMM is a general observatory type mission that can be used for a very wide variety of investigations ranging from examining solar system objects to the structure of the Universe. Also, as noted above, there is no shortage of intriguing science proposals with an oversubscription by time requested of over a factor of five.

3. Impact of past scientific results

Section 1.1 discusses the citation results for XMM. The high citation rate for papers using XMM data are impressive and demonstrates its role as a leading observatory with a strong impact on a wide variety of subjects.

4. Broad accessibility, usability, and utility of the data

All XMM data are made publicly available after a proprietary period of typically one year. There are two official archives, one at the ESA Science Operation Center (SOC) and a replicated site at the High Energy Astrophysics Science Archive Research Center (HEASARC). The HEASARC XMM archive is accessible via the standard interfaces (Browse, Xamin, and direct file transfer protocol, FTP) and is well used by both US and foreign scientists. All XMM data products are in standard Flexible Image Transport System (FITS) format, and can be analyzed by all packages designed for that format (e.g., the HEASARC HEASoft package including Xspec, Ximage, and Xronos, and the Chandra Interactive Analysis of Observations package, CIAO). XMM data can also be analyzed using HEASARC 's Hera online analysis site (§ 2.2.1), which is designed to support simultaneous multi-mission data analysis, which includes most of the Astrophysics component of the MO&DA portfolio.

Using the HEASARC infrastructure for both archiving and data analysis has been exceptionally cost effective. It also reduces the learning curve for scientists already familiar with the systems from previous observatories such as ROSAT, ASCA, and Suzaku. The GOF has supported the development of the Hera system.

5. Spacecraft and instrument health and safety.

As noted in § 2.1, the XMM observatory is in excellent health after 14 years in orbit. None of its core scientific capabilities have been compromised by either aging effects or component failures. There are no on-going concerns for observatory longevity. Demonstrating its commitment to the longevity of the XMM program, ESA in 2013 implemented a new reaction wheel control mechanism on-board the spacecraft which greatly reduces fuel usage (the only mission expendable), pushing the possible mission lifetime to ~2028.

6. Productivity and vitality of the science team

The Project Scientist, SAS programmer, and hardware team member have been part of the XMM project since before its launch in 1999. Other personnel have been with the GOF for more than half a decade providing a depth of mission understanding that benefits the community. Both as part of programmatic duties and in scientific research, GOF members have taken seriously a commitment to the community, including the teaching of university classes and collaborating with younger scientists (post-docs and graduate students). GO funds have also been extensively used for the support of younger scientists. For example, in the budget requests of the two most recent cycles, ~75% (24 out of 31) requested support for either graduate students or post-docs. A simple ADS search (XMM in the title or abstract) lists 108 Ph.D. theses based on XMM data.

7. Level and quality of observatory stewardship

From the 2012 Senior Review: "XMM is a highly capable mission in the class of the Great Observatories, offering science opportunities to the US community at low cost. The highly competitive proposal process ensures that the observatory continues to do excellent science."

Section 2.5 lists the expenses of the GOF, and demonstrates where the limited expenditure of funds is allocated. We accomplish all of the activities of listed in §2 with 2.5 FTE scientists (including the Project Scientist), one full time programmer, and <1 FTE in

other supporting staff. The GOF transitioned well into the extended mission phase with extensive cost cutting. Using 2006 funding as a conservative pre-transition support level of ~$7.5 M (some years were above $9 M), the post-transition funding of ~$2 M was a reduction of ~73%. GO funding was reduced by ~80%, severely reducing the number of graduate students and postdocs trained and qualified to analyze XMM data in the future. GOF funding was reduced by 60%. In both cases the reductions were far in excess of the 1/3 suggested in the Senior Review Call for Proposals. Even our Over-Guidelines request is well under the recommended level.

1.6 Progress report and update to activities listed in the 2012 Senior Review proposal.

As the GOF has no explicit mission science objectives the work is more completely described in the technical/budget section below.

New Work (See Section 2):

Trend data – we continue to update and enhance the utility of the Trend data including expanding the documentation and improving the ease of use of the web site.

Extended Source Analysis Software (ESAS) Image Gallery[6] – we have created the web pages and started the processing of SNRs, galaxies, and clusters of galaxies, focusing on those with multiple observations representing mosaics.

ESAS Package – we have made a number of improvements to the ESAS software including both those which are transparent to the user (e.g., conversion of all FORTRAN 77 code to Fortran 90/95 and the incorporation of the ESAS CalDB files into the SAS CCF), and which expand and simplify the range of analysis provided to the user (e.g., upgrades to allow the processing of mosaic-mode observations, the processing of MOS1 CCD #4 data after the loss of CCD #3, and reducing the number of task parameters where possible).

RGS Calibration Improvements – An improved wavelength calibration was delivered to ESA with a wavelength scale accuracy of 4 mÅ, or 60 km s^{-1} at 20 Å. In addition, an improved model for the Line Spread Function was delivered (awaiting further evaluation) which closely reproduces the measured line profiles in a number of strong emission line sources, eliminating a small discrepancy that existed previously.

Data Analysis Scripts – The GOF continues to maintain and add new data analysis scripts to our library. The scripts now include several for RGS data analysis.

6 http://heasarc.gsfc.nasa.gov/docs/xmm/xmm_gal_science.html

2012 Senior Review

"XMM is a highly capable mission in the class of the Great Observatories, offering science opportunities to the US community at low cost. The highly competitive proposal process ensures that the observatory continues to do excellent science. The SRC recommends an extension through 2016 with review in 2014, and that NASA continues funding the US GOF at their proposed levels, but increases the GO funding support to 3 million USD per year."

Maintenance (See Section 2):

Grant Support – Funds for AO-11 grants went out in 2012 October, as soon as made available by HQ. AO-12 grants are delayed until the effects of the sequester on the FY14 budget are determined.

Documentation – The ABC and D Guides to XMM data analysis have been updated for each new SAS release.

SAS – The GOF works closely with the SOC on every SAS release, which typically occur twice a year (not counting patches), particularly on the support of McIntosh operating systems.

ESAS – The ESAS CalDB files are updated as needed (e.g., with new releases of SAS).

XMM Archive – The GOF has maintained the US archive as an accurate replication of the SOC archive. It is fully interoperable with other HEASARC archives through the Browse archive interface and HERA on-line data analysis system.

OMCat – The GOF has updated the OMCat periodically as observations become publicly available, and has made the updates available through the HEASARC and the Mikulsky Archive at Space Telescope (MAST).

XMM Serendipitous Source Catalog – The master list of detected sources is updated periodically by the SOC and is incorporated promptly into the HEASARC archive.

1.7 Response to the 2012 Senior Review (SR)

From the 2012 SR report, § 9.f: *"Proposal Weaknesses: The proposal describes a minimal user support facility with limited support for funding GO science. There were no major weaknesses."* The single strongest recommendation that the 2012 SR had for the US XMM program was to request additional funds (increase support from $1 M to $3 M) for the GO grant program, leading to our over-Guidelines request for ~$4 M ($3 M for GO grants and ~$1 M for GOF operations). This additional funding, if granted, will support all US PI proposals accepted at the A/B level. The GOF can support the expanded GO program with no significant additional cost.

References

Archibald, A. M., et al. 2010, ApJ, 722, 88
Bachetti, M., et al. 2013, ApJ, 778, 163
Berghea, C. T., et al. 2013, ApJ, 776, 100
Bogdanov, S., et al. 2013, arXiv:1311.2024
Borriello, E., et al. 2012, MNRAS, 425, 1628
Branduardi-Raymont, G., et al. 2007, A&A, 463, 761
Churazov, E., et al. 2012, MNRAS, 421, 1123
Cohen, O., et al. 2011, ApJ, 733, 67
Dai, X., et al. 2012, ApJ, 755, 107
De Marco, B., et al. 2013, MNRAS, 431, 2441
de Plaa, J., et al. 2012, A&A, 539, A34
Dewey, D., et al. 2012, ApJ, 752, 103
Diaz Trigo, M., et al. 2013, Nature, in press (arXiv:1311.5080)
Done, C., et al. 2013, MNRAS, 434, 1955
Fang, M., et al. 2013, ApJS, 207, 5
Gagné, M., et al. 2011, ApJS, 194, 5
Gómez de Castro, A. I., et al. 2013, ApJ, 766, 62
Gotthelf, E. V., et al. 2013, ApJ, 765, 58
Grondin, M.-H., et al. 2012, A&A, 539, A15
Guerrero, M. A., et al. 2012, ApJ, 755, 129
Gunther, H. M., et al.2013, ApJ, 771, 70
Haberl, e. a., F. 2014, A&A., in preparation
Haberl, F., et al. 2012, A&A, 545, A128
Halpern, J. P., et al. 2013, ApJ, 753, L14
Harrison, F., et al. 2013, ApJ, 770, 103
Henley, D. B., & Shelton, R. L. 2012, ApJS, 202, 14
Henley, D. B., & Shelton, R. L. 2013, ApJ, 773, 92
Hermsen, W., et al. 2013, Science, 339, 436
Hervé, A., et al. 2013, A&A, 551, A83
Hervé, A., et al. 2012, ApJ, 748, 89
Hodges-Kluck, E. J., & Bregman, J. N. 2013, ApJ, 762, 12
Holler, M., et al. 2012, A&A, 539, A24
Humphrey, P. J., et al. 2012, ApJ, 755, 166
Kaastra, J. S., et al. 2012, A&A, 539, A117
Kara, E., et al. 2013, MNRAS, 434, 1129
Katsuda, S., et al. 2013, ApJ, 768, 182
Katsuda, S., et al. 2012a, ApJ, 756, 49
Katsuda, S., Tet al. 2012b, ApJ, 754, L7
Kavanagh, P. J., et al. 2012, A&A, 547, A19
Koutroumpa, D., et al. 2012, A&A, 545, A153
Leutenegger, M. A., et al. 2013, ApJ, 770, 80
Liu, J., et al. 2011, MNRAS, 415, L64
Liu, J., et al. 2012, MNRAS, 420, 3389
Loewenstein, M., & Davis, D. S. 2012, ApJ, 757, 121
Loewenstein, M., & Kusenko, A. 2012, ApJ, 751, 82
López-Santiago, J., et al. 2012, PASP, 124, 682
Madura, T. I., et al. 2013, MNRAS
Maggi, P., et al. 2013, ArXiv e-prints, 1310.2569
Maggi, P., et al. 2012, A&A, 548, L3
Marelli, M., et al. 2013, ApJ, 765, 36
Mereghetti, S., et al. 2013, MNRAS, 435, 2568
Mernier, F., & Rauw, G. 2013, New Astronomy, 20, 42
Miceli, M., et al. 2012, A&A, 546, A66
Miller, M. J., & Bregman, J. N. 2013, ApJ, 770, 118
Miller, N. A., et al. 2012, PASP, 124, 95
Mitsuishi, I., et al. 2013, PASJ, 65, 44
Montez, R., Jr., & Kastner, J. H. 2013, ApJ, 766, 26
Nazé, Y., et al. 2013, ApJ, 763, 143
Nebot Gómez-Morán, A., et al. 2013, A&A, 553, A12
Oskinova, L. M., et al. 2011, AN, 332, 988
Papitto, A., et al. 2013, Nature, 501, 517
Petit, V., et al. 2013, MNRAS, 429, 398
Petrucci, P.-O., et al. 2013, A&A, 549, A73
Pillitteri, I., et al. 2011, ApJ, 741, L18
Pillitteri, I., et al. 2013a, in Protostars and Planets VI, Heidelberg, July 15-20, 2013. Poster #2K057, 57
Pillitteri, I., et al. 2013b, ApJ, 768, 99
Pires, A. M., et al. 2012, A&A, 544, A17
Poppenhaeger, K., et al. 2013, ApJ, 773, 62
Pounds, K. A., & King, A. R. 2013, MNRAS, 433, 1369
Ranalli, P. 2012, AN, 333, 369
Rea, N., et al. 2012, ApJ, 754, 27
Rea, N., et al. 2013a, ApJ, 770, 65
Rea, N., et al. 2013b, arXiv:1311.3091
Read, A., et al. 2011, in The X-ray Universe 2011, ed. J.-U. Ness & M. Ehle,135
Reis, R. C., et al.2012, Science, 337, 949
Remillard, R. A., & McClintock, J. E. 2006, ARA&A, 44, 49
Risaliti, G., et al. 2013, Nature, 494, 449
Rossetti, M., et al. 2013, A&A, 556, A44
Russell, C. M. P., et al. 2013, in Massive Stars: From alpha to Omega
Sanders, J. S., & Fabian, A. C. 2012, MNRAS, 421, 726
Sanders, J. S., & Fabian, A. C. 2013, MNRAS, 429, 2727
Sanderson, A. J. R., et al. 2013, MNRAS, 429, 3288
Sasaki, M., et al. 2012, A&A, 544, A144
Saxton, R. D., et al. 2012, A&A, 541, A106
Siebeck, D., et al. 2014, Adv. Space Res., in preparation
Simionescu, A., et al. 2012, ApJ, 757, 182
Snowden, S. L., et al. 2008, A&A, 478, 615
Snowden, S. L., et al. 2009, ApJ, 691, 372
Stark, C. R., et al. 2013, ApJ, 776, 11

Sturm, R., et al. 2013, A&A, 558, A3
Su, Y., & Irwin, J. A. 2013, ApJ, 766, 61
Sundqvist, J. O., et al. 2012, MNRAS, 420, 1553
Tanaka, Y., et al. 1995, Nature, 375, 659
The Planck Collaboration et al. 2011a, A&A, 536, A9
The Planck Collaboration et al. 2011b, A&A, 536, A8
The Planck Collaboration et al. 2011c, A&A, 536, A10
The Planck Collaboration et al. 2011d, A&A, 536, A11
The Planck Collaboration et al. 2013a, A&A, 550, A130
The Planck Collaboration et al. 2013b, A&A, 550, A131
Tiengo, A., et al. 2013, Science, 500, 312
Tombesi, F., et al. 2012, MNRAS, 422, L1
Wade, G. A., et al. 2013, ArXiv e-prints, 1310.3965
Walton, D. J., et al. 2013, ApJ, 779, 148
Warwick, R. S., et al. 2012, A&A, 548, A99
Watson, M. 2012, in Half a Century of X-ray Astronomy, Proceedings of the conference held 17-21 September, 2012 in Mykonos Island, Greece (http://www.astro.noa.gr/xcosmo/, id.138)
Zhou, P., et al. 2013, arXiv:1310:7705
Zoghbi, A., et al. 2012, MNRAS, 422, 129
Zoghbi, A., et al. 2013, ApJ, 767, 12

Appendix B. Acronyms

2dF	Two Degree Galaxy and Quasar Survey
3XMM-DR4	EPIC Serendipitous Source Catalog Data Release 4
AAVSO	American Association of Variable Star Observers
AAS	American Astronomical Society
ACIS	Advanced CCD Imaging Spectrometer
ACS	Advanced Camera for Surveys
ADAP	Astrophysics Data Analysis Program
ADS	Astrophysics Data Service
AGN	Active Galactic Nuclei
AO	Announcement of Opportunity
ARK	RPS software system
ASCA	Advanced Satellite for Cosmology and Astrophysics
AXP	Anomalous X-ray Pulsar
BAL	Broad Absorption Line
BAT	Burst Alert Telescope
BGC	Bright Cluster Galaxies
BROWSE	HEASARC mission data and parameter search tool
CCD	Charge-Coupled Device
CCF	Current Calibration Files
CCO	Compact Central Object
CDM	Cold Dark Matter
Chandra	Chandra X-ray Observatory
CIE	Collisional ionization Equilibrium
CLEA	Contemporary Laboratory Experiences in Astronomy
Co-I	Co-Investigator
COR	Contracting Officer's Representative
COUP	Chandra Orion Ultradeep Project
CSM	Circumstellar Matter
CTI	Charge Transfer Inefficiency
CTTS	Classical T-Tauri Stars
CU	Columbia University
CV	Cataclysmic Variable
CWB	Colliding Wind Binaries
CXO	Chandra X-ray Observarory
DDT	Delayed Detonation
DPU	Digital Processing Unit
DROXO	Deep r Ophiuchi XMM Observation
EA	Educator Ambassadors
EPIC	European Photon Imaging Camera
EON	Extended Orion Nebula
E/PO	Education and Public Outreach
ESA	European Space Agency
ESAC	European Space Astronomy Center
ESAS	Extended Source Analysis Software
ESOC	European Space Operations Center
Fermi	Fermi Gamma-ray Space Telescope
FOV	Field of View
FTE	Full Time Equivalent
Ftools	HEASARC multi-mission data analysis software package
FUV	Far Ultraviolet
FWHM	Full Width at Half Maximum
FY	Fiscal Year
GALEX	Galaxy Evolution Explorer

GBH	Galactic Black Hole
GLAST	Gamma-ray Large Area Space Telescope
GO	Guest Observer
GOF	NASA/GSFC Guest Observer Facility
GPG	Public domain version of Pretty Good Privacy
GRB	Gamma-Ray Burst
GSFC	Goddard Space Flight Center
GT	Guaranteed Time
GTN	Global Telescope Network
HEASARC	High Energy Astrophysics Science Archive Research Center
HEASoft	HEASARC data reduction and analysis software package
HESS	High Energy Stereoscopic System
HERA	HEASARC multi-mission interactive data analysis facility
Herschel	Herschel Space Observatory
HETG	High Energy Transmission Grating
HPD	Half Power Diameter
HST	Hubble Space Telescope
IACHEC	International Consortium for High-Energy Calibration
ICM	Intracluster Medium
IGM	Intergalactic Medium
IMBH	Intermediate Mass Black Hole
INS	Isolated Neutron Stars
INTEGRAL	International Gamma-Ray Astrophysics Laboratory
IR	Infra Red
IRAS	Infra Red Astronomical Satellite
ISM	Interstellar Medium
ITEA	International Technology Education Association
IYA	International Year of Astronomy
JPL	Jet Propulsion Laboratory
LANL	Los Alamos National Laboratory
LBV	Luminous Blue Variables
ΛCDM	Lambda Cold Dark Matter
LETG	Low Energy Transmission Grating
LMC	Large Magellanic Cloud
LMXB	Low Mass X-ray Binary
LP	Large Programs
LTI	Learning Technologies, Inc.
LTSA	Long Term Support in Astrophysics
MAST	Mikulski Archive at Space Telescope
MCELS	Magellanic Cloud Emission Line Survey
MESA	Math, Engineering, Science, Achievement
MOO	Mission of Opportunity
MOS	MOS style EPIC CCD detector
MSP	Millisecond Pulsar
MSSL	Mullard Space Science Laboratory
NAG	Numerical Algorithms Group
NAS	National Academy of Sciences
NASA	National Aeronautics and Space Administration
NLS1	Narrow Line Seyfert 1
NPS	North Polar Spur
NRC	National Research Council
NS	Neutron Star
NSF	National Science Foundation
NuSTAR	Nuclear Spectroscopic Telescope Array
NVO	National Virtual Observatory

OM	Optical Monitor
OMCat	Optical Monitor Source Catalog
OSS	Office of Space Science
PDS	Power Density Spectrum
PGP	Pretty Good Privacy
PHS	Planet Hosting Star
PI	Principal Investigator
PIMMS	Portable, Interactive Multi-Mission Simulator
Planck	An ESA microwave space observatory
PMO	Primary Mission Objectives
PMS	Pre Main Sequence
PN	PN style EPIC CCD detector
PNe	Planetary Nebulae
PSD	Power Spectral Density
PSF	Point Spread Function
PV	Pointing Verification
PWN	Pulsar Wind Nebula
QPO	Quasi-Periodic Oscillation
QSO	Quasi-Stellar Object
RASS	ROSAT All-Sky Survey
RCS	Resonant Cyclotron Scattering
REXCESS	Representative XMM-Newton Cluster Structure Survey
RGA	Reflection Grating Array
RGS	Reflection Grating Spectrometer
RMS	Root Mean Square
ROSAT	Rontgen Satellite
RPS	Remote Proposal System
RXTE	Rossi X-ray Time Explorer
SAS	Science Analysis System
SDSS	Sloan Digital Sky Survey
SED	Spectral Energy Distribution
SEU	Structure and Evolution of the Universe
SGR	Soft Gamma-ray Repeater
SMBH	Supermassive Black Hole
SMC	Small Magellanic Cloud
SMD	Science Mission Directorate
SMEX	Small Explorer
SN	Supernova
SNe	Supernovae
S/N	Signal to Noise
SNR	Supernova Remnant
SOC	Science Operations Center
SOS	Survey of Orion A with XMM and Spitzer
SPI	Star-Planet Interactions
Spitzer	Spitzer Space Telescope
SRON	Netherlands Institute for Space Research
SSB	Space Studies Board (of the NRC)
SSC	Survey Science Centre
SSSC	Slew Survey Source Catalog
SSU	Sonoma State University
STEM	Science, Technology, Engineering and Math
STScI	Space Telescope Science Institute
Suzaku	Suzaku X-ray Telescope
SWCX	Solar Wind Charge Exchange
Swift	Swift Gamma-Ray Burst Mission

SWIRE	Spitzer Wide-area Infrared Extragalactic Survey
SZ	Sunyaev-Zel'dovich
TAX	Two-Absorber X-ray
TAXP	Transient Anomalous X-ray Pulsar
TD	Thermal Dominant
ToO	Target of Opportunity
UFO	Ultra Fast Outflow
UK	United Kingdom
ULX	Ultra-Luminous X-ray source
UMCP	University of Maryland-College Park
US	United States
USNO	US Naval Observatory
UV	Ultra Violet
UVES	Ultraviolet and Visual Echelle Spectrograph
VERITAS	Very Energetic Radiation Imaging Telescope Array System
VLP	Very Large Program
VLT	Very Large Telescope
WHIM	Warm Hot Intercluster Medium
WN	Nitrogen sequence subclass of Wolf-Rayet stars
WR	Wolf-Rayet
XCS	X-ray Cluster Survey
XDINS	X-ray Dim Isolated Neutron Stars
XEST	XMM-Newton Extended Survey of Taurus
XID	X-ray source IDenfication program
XMM	XMM-Newton
XMM-Newton	Newton X-ray Multi-Mirror Observatory
XMM-ESAS	XMM-Newton Extended Source Analysis Software
XRB	X-ray Binary
XSA	XMM-Newton Science Archive
XXL Survey	Extra Extra Large Survey
YSO	Young Stellar Object

Appendix C. Online Bibliography

The XMM bibliography (a GOF product) can be found at:
http://heasarc.gsfc.nasa.gov/docs/xmm/xmmbib.html